Adaptive GDSW Coarse Spaces of Reduced Dimension for Overlapping Schwarz Methods

Heinlein, Alexander; Klawonn, Axel; Knepper, Jascha; Rheinbach, Oliver; Widlund, Olof B.

DOI
10.1137/20M1364540

Publication date
2022

Document Version
Final published version

Published in
SIAM Journal on Scientific Computing

SIAM J. SCI. COMPUT.
Vol. 44, No. 3, pp. A1176–A1204

ADAPTIVE GDSW COARSE SPACES OF REDUCED DIMENSION FOR OVERLAPPING SCHWARZ METHODS*

ALEXANDER HEINLEIN†, AXEL KLAWONN‡§, JASCHA KNEPPER‡,
OLIVER RHEINBACH¶, AND OLOF B. WIDLUND‖

Abstract. A new reduced-dimension adaptive generalized Dryja–Smith–Widlund (GDSW) overlapping Schwarz method for linear second-order elliptic problems in three dimensions is introduced. It is robust with respect to large contrasts of the coefficients of the partial differential equations. The condition number bound of the new method is shown to be independent of the coefficient contrast and only dependent on a user-prescribed tolerance. The interface of the nonoverlapping domain decomposition is partitioned into nonoverlapping patches. The new coarse space is obtained by selecting a few eigenvectors of certain local eigenproblems which are defined on these patches. These eigenmodes are energy-minimally extended to the interior of the nonoverlapping subdomains and added to the coarse space. By using a new interface decomposition, the reduced-dimension adaptive GDSW overlapping Schwarz method usually has a smaller coarse space than existing GDSW and adaptive GDSW domain decomposition methods. A robust condition number estimate is proven for the new reduced-dimension adaptive GDSW method which is also valid for existing adaptive GDSW methods. Numerical results for the equations of isotropic linear elasticity in three dimensions confirming the theoretical findings are presented.

Key words. domain decomposition, multiscale, GDSW, overlapping Schwarz, adaptive coarse spaces, reduced dimension

AMS subject classifications. 65F08, 65F10, 65N55, 68W10

DOI. 10.1137/20M1364540

1. Introduction.

Successful domain decomposition preconditioners for solving elliptic problems in general require at least one global, coarse-level component in order to perform satisfactorily if the number of subdomains into which the given domain has been decomposed is relatively large. The design and analysis of these coarse components is central in most studies in this field given that they require global communication if the algorithms are implemented on distributed or parallel computing systems. In order to avoid creating a bottleneck, it is very important to keep the dimension of the related coarse space small.

In recent years, substantial progress has been possible by the development of algorithms which adaptively design the coarse space at a cost of solving local generalized eigenvalue problems. In this paper, we will focus on a particular family of domain

*Submitted to the journal's Methods and Algorithms for Scientific Computing section September 4, 2020; accepted for publication (in revised form) October 4, 2021; published electronically May 9, 2022.

https://doi.org/10.1137/20M1364540

Funding: This work was supported by the DFG through grant DFG FKZ: INST 216/512/1FUGG.

†Delft Institute of Applied Mathematics, Delft University of Technology, Delft, 2628 CD, The Netherlands (a.heinlein@tudelft.nl)

‡Department of Mathematics and Computer Science, University of Cologne, 50931 Köln, Germany (axel.klawonn@uni-koeln.de, jascha.knepper@uni-koeln.de, http://www.numerik.uni-koeln.de).

§Center for Data and Simulation Science, University of Cologne, 50931 Köln, Germany (http://www.cds.uni-koeln.de).

¶Institut für Numerische Mathematik und Optimierung, Fakultät für Mathematik und Informatik, Technische Universität Freiberg, 09599 Freiberg, Germany (oliver.rheinbach@math.tu-freiberg.de, http://www.mathe.tu-freiberg.de/nmo/mitarbeiter/oliver-rheinbach).

‖Department of Mathematics, Courant Institute, New York, NY 10012 USA (widlund@cims.nyu.edu, https://cs.nyu.edu/faculty/widlund).

decomposition algorithms, the two-level overlapping Schwarz methods, which use one coarse-level component in addition to local components each of which is defined on a subdomain which is part of an overlapping decomposition. We note that the use of adaptively designed coarse spaces has been very successful even with problems with very irregular coefficients; this is clearly demonstrated by examples in section 14 of this paper.

The robustness of many coarse spaces for arbitrary coefficient functions is obtained by using local generalized eigenvalue problems to adaptively enrich the coarse spaces with suitable basis functions; see, e.g., [15, 45, 10, 47, 16, 22, 14]. These approaches differ, e.g., in the sizes of the eigenvalue problems, the coarse space dimensions, the class of problems considered, and their parallel efficiency. We also mention success with adaptive coarse spaces for nonoverlapping domain decomposition methods; see, e.g., [2, 39, 40, 48, 42, 33, 35, 43, 32, 34, 41].

Two-level overlapping Schwarz algorithms were first developed with coarse spaces based on a coarse triangulation of the domain and with subdomains obtained by adding one or a few layers of fine elements to each coarse mesh element; see [49, Chapter 3]. In contrast, the iterative substructuring algorithms, developed for decompositions of the domain into nonoverlapping subdomains, were immediately available for quite irregular subdomains such as those obtained by a mesh partitioner such as METIS [31]; see [49, Chapters 4–6]. The iterative substructuring algorithms have been very successful, but they cannot be used unless submatrices associated with the subdomains are available instead of just a fully assembled stiffness matrix. This was a main reason why a new family of overlapping Schwarz algorithms was developed, known as the generalized Dryja–Smith–Widlund (GDSW) methods, which borrow their coarse components from [49, Algorithm 5.16]. These ideas were first developed in [5, 6]. The elements of these coarse spaces are defined by their values on the interface between the subdomains with values in the interiors defined by energy-minimizing extensions. These algorithms were further developed for almost incompressible elasticity in two papers [7, 8]; in the second paper, the dimension of the coarse spaces was considerably decreased; see also [25, 18, 26, 27, 19, 24, 28] for further developments.

In this paper, we present an approach of constructing adaptive coarse spaces for the two-level overlapping Schwarz method [46, 49] based on the adaptive GDSW (AGDSW) coarse space of [23]. In particular, our focus is on one new coarse space—the reduced-dimension adaptive GDSW (RAGDSW) coarse space—and the reduction of the coarse space dimension. We remark that, in contrast to GDSW, adaptive GDSW-type coarse spaces do require subdomain matrices resulting from subdomain problems with Neumann boundary conditions. A proof of a condition number estimate, which is independent of heterogeneities of the coefficient functions, is given in sections 10 and 11. We note that this proof is based on a more general decomposition of the interface than the one in [23]; this proof works for both the original AGDSW and the new RAGDSW coarse space. Supporting numerical results are presented in section 14.

In our adaptive algorithms, a user-prescribed tolerance directly controls the condition number of the preconditioned operator, and if this tolerance is chosen as zero, adaptive GDSW is identical to GDSW and reduced-dimension adaptive GDSW identical to reduced-dimension GDSW, the latter being a variant of GDSW defined on a specific interface partition of the domain decomposition; cf. section 8.

We note that our reduced-dimension GDSW coarse space differs from the reduced-dimension GDSW coarse spaces in [9]. However, they share the same core idea: GDSW and AGDSW use basis functions associated with coarse nodes, edges, and

faces, while the coarse spaces in [9], reduced-dimension GDSW, and reduced-dimension adaptive GDSW use basis functions associated only with subdomain vertices. Generally, this leads to a reduction in the coarse space dimension. See also [8, 4, 29, 20] for reduced-dimension GDSW coarse spaces.

We note that many other approaches to constructing coarse spaces exist. Some borrow the idea from the multiscale finite element method (MsFEM) [30, 13] and use basis functions of that type in or for the construction of the coarse space; cf. [1, 17, 12, 3, 16, 22, 14]. However, the coarse spaces in this paper are not based on MsFEM functions.

The outline of the paper is as follows. In section 2, we introduce our model problem followed by the definition of the two-level additive overlapping Schwarz methods in section 3. In the following five sections, we introduce four families of GDSW algorithms. In section 9, we give a quite general description of adaptive GDSW coarse spaces which covers both adaptive GDSW and reduced-dimension adaptive GDSW; see also section 12 for a variant which is computationally cheaper, easier to implement, and more efficient in a parallel implementation. In sections 10 and 11, we derive a condition number estimate for our new reduced-dimension adaptive GDSW preconditioner. In section 13, we address questions that may arise about the implementation due to encountering singular matrices for certain extension operators described in section 9. Finally, in section 14, we present numerical results for a selection of coefficient functions.

For the reader's convenience, an overview of some definitions is given in Table 1.

TABLE 1
Reference table for some definitions used in this paper (in order of their appearance).

Description of coarse spaces (sections 4 – 8)		
x^h	finite element node	section 4
$\mathcal{P}$	nonoverlapping partition of the interface	section 4
$\overline{\Omega}_\xi$	union of the closure of the subdomains adjacent to a $\xi \in \mathcal{P}$	section 5
$\{\xi_i\}_{i=1}^{n_\xi}$	partitioning of a $\xi \in \mathcal{P}$ into nodal equivalence classes	
	structured mesh, structured domain decomposition	eq. (7.1)
	unstructured mesh, unstructured domain decomposition	section 8
$n(x^h)$	index set of subdomains which contain x^h	eq. (8.1)
Theory (sections 9 – 11)		
n^ξ	index set of subdomains adjacent to a $\xi \in \mathcal{P}$	eq. (9.1)
$z_{\xi\to G}(\cdot)$	extension by zero from ξ to G	eq. (9.2)
$X^h(\xi)$	finite element space associated with a set of nodes ξ	section 9
$\mathcal{H}_{\xi\to\Omega_\xi}(\cdot)$	energy-minimizing extension from ξ to Ω_ξ	eq. (9.3)
$c_\xi(u,v)$	$c_\xi(u,v) := \sum_{i=1}^{n_\xi} c_{\xi_i}(u,v)$	eq. (9.4)
$c_{\xi_i}(u,v)$	$c_{\xi_i}(u,v) := a_{\Omega_{\xi_i}}(z_{\xi_i\to\Omega_{\xi_i}}(u), z_{\xi_i\to\Omega_{\xi_i}}(v))$	eq. (9.5)
$\|u\|^2_{c_\xi}$	$\|u\|^2_{c_\xi} := c_\xi(u,u)$	eq. (9.6)
$\Pi_\xi w$	$\Pi_\xi := \sum_{\lambda_{k,\xi}\le tol_\xi} c_\xi(w, v_{k,\xi}) v_{k,\xi}$	eq. (10.1)
$\Pi_\mathcal{P} w$	$\Pi_\mathcal{P} w := \sum_{\xi\in\mathcal{P}} \Pi_\xi w$	eq. (10.1)
$\|u\|_{d_\xi}$	$\|u\|_{d_\xi} := \sqrt{d_\xi(u,u)}, \quad d_\xi(\cdot,\cdot) := a_{\Omega_\xi}(\mathcal{H}_{\xi\to\Omega_\xi}(\cdot), \mathcal{H}_{\xi\to\Omega_\xi}(\cdot))$	eq. (10.2)
$\|u\|_{a(B)}$	$\|u\|_{a(B)} := \sqrt{a_B(u,u)}$	eq. (10.3)
C_τ	max. number of vertices of a finite element	Lemma 11.2
$\mathcal{P}(\Omega_i)$	$\xi \in \mathcal{P}$ adjacent to subdomain i	eq. (11.1)
N^ξ	max. number of $\xi \in \mathcal{P}$ adjacent to a subdomain	eq. (11.1)
$tol_\mathcal{P}$	$tol_\mathcal{P} := \min_{\xi\in\mathcal{P}} tol_\xi$	Lemma 11.2
$\mathcal{N}_{ec,\mathcal{P}}$	$\mathcal{N}_{ec,\mathcal{P}} := \bigcup_{\xi\in\mathcal{P}} \{\xi_i, i = 1,\dots,n_\xi\}$	eq. (11.3)
$\mathcal{C}$	measure for the $\mathcal{P}$-connectivity of the domain decomposition	eq. (11.5)

2. Linear elasticity. We will consider a variational formulation of the equations of compressible linear elasticity: Find $u \in \left(H_0^1(\Omega)\right)^3$ such that

$$a_\Omega(u,v) = L(v) \qquad \forall v \in \left(H_0^1(\Omega)\right)^3, \tag{2.1}$$

where $\Omega \subset \mathbb{R}^3$ is a polyhedral domain and

$$a_\Omega(u,v) := \int_\Omega 2\mu(x)\Big(\varepsilon(u(x)) : \varepsilon(v(x))\Big)\,dx + \int_\Omega \lambda(x)\Big(\operatorname{div}(u(x))\operatorname{div}(v(x))\Big)\,dx,$$
$$L(v) := \int_\Omega f(x)v(x)\,dx.$$

The Lamé parameters $0 < \lambda(x),\ \mu(x) \colon \mathbb{R}^3 \to \mathbb{R}$ are scalar coefficient functions, $f \in \left(L^2(\Omega)\right)^3$,

$$\varepsilon(u) := \tfrac{1}{2}\Big(\nabla u + \big(\nabla u\big)^T\Big)$$

and

$$A : B := \operatorname{tr}(A^T B) = \sum_{i,j=1}^{3} A_{ij}B_{ij},$$

for any matrices $A, B \in \mathbb{R}^{3\times 3}$.

We will consider problems with a highly heterogeneous Young modulus $E \colon \Omega \to \mathbb{R}$, $0 < E_{\min} \le E(x) \le E_{\max}$, and a positive Poisson ratio ν, bounded away, from above, by $1/2$, and we define the Lamé parameters by

$$\lambda(x) := \frac{E(x)\nu}{(1+\nu)(1-2\nu)}, \qquad \mu(x) := \frac{E(x)}{2(1+\nu)}.$$

The algorithms described in this paper can also be applied to other linear, second-order elliptic problems including those in two dimensions.

Let $\tau_h := \tau_h(\Omega)$ be a finite element discretization of Ω. We will use a conforming space $V^h(\Omega)$ of piecewise linear or trilinear finite elements on this mesh and for simplicity assume that the Lamé parameters are constant on each element $T \in \tau_h$.

We will use the conjugate gradient method preconditioned by two-level overlapping Schwarz methods to solve the resulting linear system $Ku = b$. Here K is the stiffness matrix obtained from the bilinear form $a_\Omega(\cdot,\cdot)$ and the finite element space $\mathring{V}^h(\Omega) := V^h(\Omega) \cap \left(H_0^1(\Omega)\right)^3$.

For completeness, we note that the Dirichlet boundary condition has been incorporated into the global stiffness matrix by setting those rows and columns of K to unit vectors that correspond to Dirichlet boundary nodes.

3. Two-level overlapping Schwarz methods. We will now introduce the two-level Schwarz algorithms, mostly following [49, Chapter 2.2]. The different variants considered in this paper will differ in the coarse space chosen; the design of the coarse space is the main issue in this study and many other studies of algorithms of this kind. In the next five sections, we will introduce four different variants. In section 12, we also explore alternatives that decrease the costs of using the two algorithms that use adaptive choices of their coarse spaces.

We partition the domain Ω into N nonoverlapping subdomains Ω_i with a maximum diameter H, each a union of finite elements, and denote the corresponding interface by $\Gamma := \bigcup_{i\neq j} (\partial\Omega_i \cap \partial\Omega_j) \setminus \partial\Omega$. We extend each subdomain Ω_i by k layers of

finite elements to obtain an overlapping domain decomposition $\{\Omega_i'\}_{i=1}^N$ and introduce local spaces $V_i, i \in \{1, 2, \ldots, N\}$ as the subspaces of elements of $V^h(\Omega_i')$, which vanish on $\partial\Omega_i'$, that is, $V_i := \mathring{V}^h(\Omega_i') := V^h(\Omega_i') \cap \left(H_0^1(\Omega_i')\right)^3$.

Associated with each such subdomain is a restriction operator $R_i : \mathring{V}^h(\Omega) \to V_i$ and an extension operator $R_i^T : V_i \to \mathring{V}^h(\Omega)$. Furthermore, for any global coarse space $V_0 \subset \mathring{V}^h(\Omega)$, we define a linear interpolation operator $R_0 : \mathring{V}^h(\Omega) \to V_0$, where each of the columns of the matrix R_0^T represents a coarse basis function defined on the fine mesh τ_h.

We will use exact solvers for all the subspaces defined in terms of bilinear forms on V_i, $i \in \{0, 1, \ldots, N\}$, given by

$$\tilde{a}_i\left(u_i, v_i\right) = a_\Omega\left(R_i^T u_i, R_i^T v_i\right) \quad \forall u_i, v_i \in V_i;$$

cf. [49, Chapter 2.2]. The associated matrices are given by $K_i = R_i K R_i^T$, $i = 0, 1, \ldots, N$. The additive one-level Schwarz preconditioned operator is given by $P_{\text{OS-1}} = \sum_{i=1}^N R_i^T K_i^{-1} R_i K$ and that of the additive two-level Schwarz operator by

$$P_{\text{OS-2}} = R_0^T K_0^{-1} R_0 K + P_{\text{OS-1}}.$$

4. The GDSW preconditioner. In what follows, x^h will denote a finite element node. Those on the interface form the set $\Gamma^h := \{x^h \in \Gamma\}$. A key ingredient of each of our coarse spaces is a partition $\mathcal{P}$ of Γ^h into disjoint interface components $\xi^h \subset \Gamma^h$ such that

$$\Gamma^h = \bigcup_{\xi^h \in \mathcal{P}} \xi^h.$$

To simplify, we will omit the superscript h and write ξ instead of ξ^h.

The GDSW [5, 6], AGDSW [21, 23], RGDSW [9, 29] (see also section 6), and RAGDSW (see section 7) preconditioners are two-level overlapping Schwarz methods, and their preconditioners can be written in matrix form as

$$M^{-1} = \Phi\left(\Phi^T K \Phi\right)^{-1} \Phi^T + \sum_{i=1}^N R_i^T K_i^{-1} R_i.$$

The basis functions of all our coarse spaces, i.e., the columns of $\Phi = R_0^T$, are defined by an energy-minimizing extension of the values Φ_Γ on the interface Γ^h to the subdomains, i.e., by

$$\Phi = \begin{bmatrix} \Phi_I \\ \Phi_\Gamma \end{bmatrix} = H_\Gamma \Phi_\Gamma, \quad H_\Gamma := \begin{bmatrix} -K_{II}^{-1} K_{I\Gamma} \\ I_\Gamma \end{bmatrix}. \tag{4.1}$$

Here I_Γ is the identity matrix on Γ^h and H_Γ is constructed from submatrices of the global stiffness matrix

$$K := \begin{bmatrix} K_{II} & K_{I\Gamma} \\ K_{\Gamma I} & K_{\Gamma\Gamma} \end{bmatrix},$$

where I refers to the set of variables not associated with the interface. We note that I also contains boundary nodes of Ω. From the definition follows that Φ is zero on the domain boundary (cf. Remark 8.1). We note that K_{II} is block-diagonal and that $K_{\Gamma I} = K_{I\Gamma}^T$ also can be written in block form as

$$K_{II} = \begin{bmatrix} K_{II}^{(1)} & & \\ & \ddots & \\ & & K_{II}^{(N)} \end{bmatrix}, K_{\Gamma I} = \begin{bmatrix} K_{\Gamma I}^{(1)} & \ldots & K_{\Gamma I}^{(N)} \end{bmatrix}.$$

The superscripts of these matrices mark contributions from the subdomains Ω_i to the stiffness matrix K.

Given the sparsity of the stiffness matrix, reflecting the local coupling of the variables, all these matrix blocks are sparse, and the coarse space basis functions are each associated only with a few subdomains. In the original GDSW method for the scalar two-dimensional case, the columns of Φ_Γ are given by the characteristic functions of vertices and subdomain edges; i.e., the interface is partitioned as follows: $\Gamma^h = \left(\bigcup_{v\in\mathcal{V}} v\right) \cup \left(\bigcup_{e\in\mathcal{E}} e\right)$, where $\mathcal{V}$ and $\mathcal{E}$ are the sets of nodes of the subdomain vertices and subdomain edges, respectively; cf. Figure 1 (top left) for the interface partition and (top right) for two corresponding coarse functions. For the three-dimensional case, the basis functions are defined analogously, using characteristic functions for interface vertices, edges, and faces.

In more general cases, the boundary values on Γ span the restriction of the null space of K^N to Γ, where K^N is the stiffness matrix given by $a_\Omega(\cdot,\cdot)$ with a Neumann boundary condition on $\partial\Omega$. Thus, for example, in the case of linear elasticity in three dimensions and any subdomain edge which is not straight, we obtain 6 functions: 3 translations and 3 linearized rotations. We note that the restriction of the rigid body modes to a straight edge are linearly dependent; see [7].

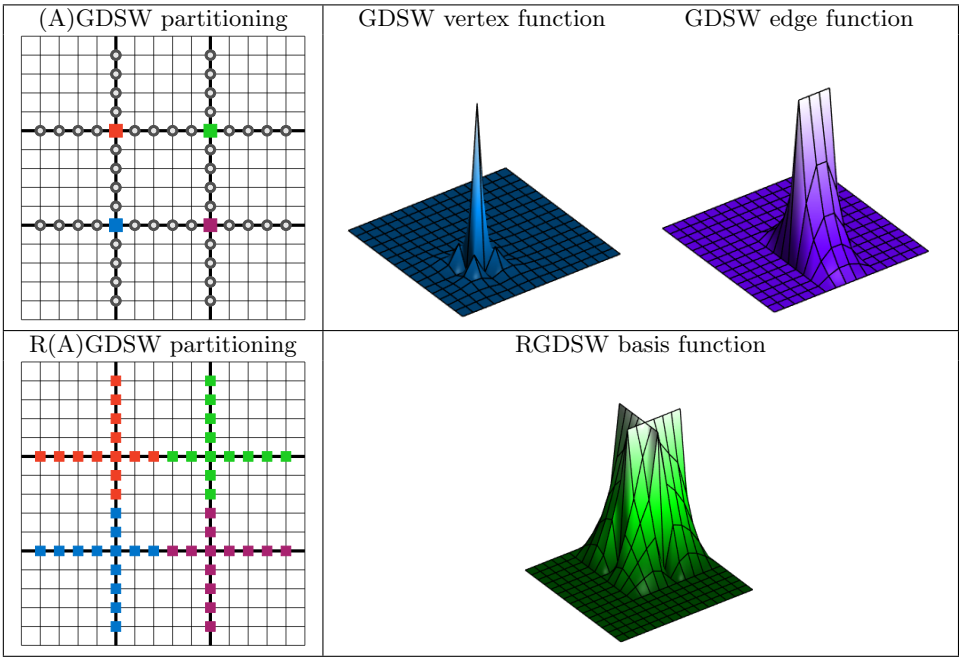

FIG. 1. *Left: Decomposition of the interface Γ^h. Top Left: Decomposition of Γ^h into 16 components: 4 vertices and 12 edges (with 4 nodes each) as used in the GDSW and adaptive GDSW method. Bottom Left: Decomposition of Γ^h into 4 components as used in the reduced-dimension GDSW and reduced-dimension adaptive GDSW methods. Right: Corresponding coarse functions for a two-dimensional diffusion problem are shown on the right for GDSW (top) and RGDSW (bottom). Homogeneous Dirichlet boundary conditions are assumed on $\partial\Omega$. The GDSW vertex function (top center) corresponds to the blue vertex. The GDSW edge function (top right) corresponds to the edge between the blue and magenta vertices. The RGDSW coarse function (bottom right) corresponds to the green component.*

The matrix of the GDSW coarse operator can be computed either by forming the triple matrix product $\Phi^T K \Phi$ or by exploiting the fact that

$$\Phi^T K \Phi = \begin{bmatrix} -K_{II}^{-1} K_{I\Gamma} \Phi_\Gamma \\ \Phi_\Gamma \end{bmatrix}^T \begin{bmatrix} K_{II} & K_{I\Gamma} \\ K_{\Gamma I} & K_{\Gamma\Gamma} \end{bmatrix} \begin{bmatrix} -K_{II}^{-1} K_{I\Gamma} \Phi_\Gamma \\ \Phi_\Gamma \end{bmatrix} = \Phi_\Gamma^T S_{\Gamma\Gamma} \Phi_\Gamma,$$

where $S_{\Gamma\Gamma} = K_{\Gamma\Gamma} - K_{\Gamma I} K_{II}^{-1} K_{I\Gamma}$ is the Schur complement obtained by eliminating the interior variables of all subdomains and those on the boundary of Ω.

Energy-minimizing extensions play a fundamental role for domain decomposition methods. Note that in case of a bilinear form defined by the Laplace operator, an energy-minimizing extension reduces to a harmonic extension. We refer the reader to [49, section 4.4] for a discussion of discrete harmonic extensions.

It is well known that, in general, to obtain a scalable method, the coarse space must be able to represent the null space [46, 49]. By restricting the null space to a partition of the interface and then extending it energy-minimally, we fulfill the above criterion.

5. Standard adaptive GDSW coarse space. The standard adaptive GDSW method, the AGDSW method, uses the same interface partitioning $\mathcal{P}$, based on subdomain vertices, edges, and faces, as the GDSW method. The coarse functions for the vertices are the same as for the GDSW variant, but the columns of Φ corresponding to the edges and faces are not. Instead, we use a few of the eigenfunctions of local generalized eigenvalue problems of the form

$$S_{\xi\xi} \tau_{*,\xi} = \lambda_{*,\xi} K_{\xi\xi}^{\Omega_\xi} \tau_{*,\xi}, \tag{5.1}$$

where ξ corresponds to an edge or a face.

The particular problem (5.1) was introduced in [23]; it is the main goal of this work to modify the right-hand side of (5.1) to allow more general interface decompositions; see sections 6 and 7.

To define the Schur complement $S_{\xi\xi}$ and the matrix $K_{\xi\xi}^{\Omega_\xi}$, for any edge and face ξ, we will use the local stiffness matrix K^{Ω_ξ} on Ω_ξ with Neumann boundary conditions. Here $\overline{\Omega}_\xi$ is the closure of the union of all subdomains which are adjacent to ξ and $\Omega_\xi := \overline{\Omega}_\xi \setminus \partial\Omega_\xi$ its interior. The stiffness matrix K^{Ω_ξ} is defined by $a_{\Omega_\xi}(\cdot,\cdot)$ and can be assembled from the subdomain stiffness matrices of the subdomains adjacent to the edge or face.

We note that, for this type of eigenvalue problem, the Neumann boundary condition is essential to construct a robust preconditioner. For the proof of Lemma 10.2, this condition is required to be able to use an energy-minimizing property; see below and (10.4). Therein, a spectral estimate allows us to bound (contrast independently) a high-energy term using a low-energy term, which is reflected by the fact that $\tau^T S_{\xi\xi} \tau \leq \tau^T K_{\xi\xi}^{\Omega_\xi} \tau$; cf. sections 9 and 10. If, on the other hand, a zero Dirichlet boundary condition were used (i.e., introducing a forced slope to zero), the coarse space would not be robust for high-coefficient components that intersect multiple interface components.

We partition the degrees of freedom of $\overline{\Omega}_\xi$ into the set associated with ξ and the rest which forms a set R and write the stiffness matrix as

$$K^{\Omega_\xi} = \begin{pmatrix} K_{RR}^{\Omega_\xi} & K_{R\xi}^{\Omega_\xi} \\ K_{\xi R}^{\Omega_\xi} & K_{\xi\xi}^{\Omega_\xi} \end{pmatrix}$$

and can then define the Schur complement by

$$S_{\xi\xi} := K_{\xi\xi}^{\Omega_\xi} - K_{\xi R}^{\Omega_\xi}\left(K_{RR}^{\Omega_\xi}\right)^{+} K_{R\xi}^{\Omega_\xi},$$

where $\left(K_{RR}^{\Omega_\xi}\right)^{+}$ is a pseudoinverse of $K_{RR}^{\Omega_\xi}$; see Remark 9.1 and section 13 for more details. The Schur complement originates from the application of K^{Ω_ξ} and an energy-minimizing extension from ξ to Ω_ξ; cf. (9.3) and (9.7). For our elasticity problems, K^{Ω_ξ} as well as $S_{\xi\xi}$ will be singular.

We sort the eigenvalues of (5.1) in nondescending order, i.e., $0 = \lambda_{1,\xi} \leq \lambda_{2,\xi} \leq ... \leq \lambda_{m,\xi}$, where m is the number of unknowns of (5.1). We select all eigenvectors $\tau_{*,\xi}$ with eigenvalues smaller than or equal to a certain threshold, i.e., $\lambda_{*,\xi} \leq tol_\xi$, and then define $\tau_{*,\Gamma}$ as the extension by zero of $\tau_{*,\xi}$ from ξ to Γ^h. The coarse basis functions corresponding to ξ are then the extensions

$$v_{*,\xi} := H_\Gamma \tau_{*,\Gamma},$$

and the columns of Φ are now given by the $v_{*,\xi}$, selected, and the GDSW vertex functions.

Remark 5.1. If $tol_\xi = 0$ for all $\xi \in \mathcal{P}$, the AGDSW coarse space contains only the coarse functions associated with the null space of the Schur complement $S_{\xi\xi}$. The latter is identical to the null space of K^{Ω_ξ} restricted to ξ. Thus, in this case, AGDSW reduces to GDSW, and we have

$$V_{\mathrm{GDSW}} = V_{\mathrm{AGDSW}}^0 \subset V_{\mathrm{AGDSW}}^{tol(\mathcal{P})}.$$

$V_{\mathrm{AGDSW}}^{tol(\mathcal{P})}$ is the AGDSW coarse space allowing individual tolerances tol_ξ, $\xi \in \mathcal{P}$. Accordingly, for V_{AGDSW}^0, we have $tol_\xi = 0$ for all $\xi \in \mathcal{P}$. See also Remark 7.1.

Let $tol_{\mathcal{E}}$ and $tol_{\mathcal{F}}$ be the smallest tolerance used for the subdomain edges and faces, respectively. For positive tolerances, the following condition number estimate for the preconditioned operator has been derived previously for scalar diffusion problems; see [23, Corollary 6.6].

THEOREM 5.2. *The condition number of the AGDSW two-level Schwarz operator in three dimensions is bounded by*

$$\kappa(M_{\mathrm{AGDSW}}^{-1} K) \leq \left(20 + \frac{34(N^{\mathcal{E}})^2 n_{max}^{\mathcal{E}}}{tol_{\mathcal{E}}} + \frac{68(N^{\mathcal{F}})^2}{tol_{\mathcal{F}}}\right)\left(\hat{N}_c + 1\right).$$

The constant $\hat{N}_c$ is an upper bound of the number of overlapping subdomains that any point $x^h \in \Omega$ can belong to. $N^{\mathcal{E}}$ and $N^{\mathcal{F}}$ are the maximum number of subdomain edges and faces, respectively, of any subdomain. $n_{max}^{\mathcal{E}}$ is the maximum number of subdomains that share a subdomain edge. All constants are independent of H, h, and the contrast of the coefficient function.

This kind of result also holds for linear elasticity; see Theorem 11.5 and section 11.

6. A reduced-dimension GDSW coarse space. We will first give a simple description of an interface partition for a structured mesh and domain decomposition. This partition can also be used for the reduced-dimension adaptive GDSW coarse spaces.

Our goal is to reduce the number of interface components, as this leads to a smaller coarse space dimension. Note that for the adaptive variants, in case of a

highly heterogeneous coefficient function, the coarse space dimension may not always be smaller. To this end, each vertex of the coarse mesh will be associated with an interface component ξ formed by parts of the edges and faces adjacent to the vertex. A disjoint partition is obtained by distributing parts of these faces and edges equally or almost equally between nearby vertices; see Figure 1 (bottom left) for a two-dimensional representation in which the number of interface components is reduced from 16 (GDSW) to 4 (RGDSW). Note that for GDSW-type coarse spaces, the dimension of the coarse space is lower than or equal to the number of interface components multiplied with the dimension of the null space of K^N; cf. section 4.

The reduced-dimension GDSW coarse space is then defined completely analogously to the GDSW coarse space. Thus, the restriction of the null space elements to the interface components is first extended by zero to the rest of the interface nodes and then extended with minimal energy to the subdomain interiors to obtain the coarse functions; see Figure 1 (bottom right) for one of the coarse functions for a two-dimensional diffusion problem.

We note that our RGDSW coarse space differs from those of [9] but can be regarded as a variant of the coarse spaces introduced in that paper.

7. The reduced-dimension adaptive GDSW coarse space. For the reduced adaptive GDSW coarse space, we need to partition each interface component ξ, as those of the previous section, into subcomponents. For a structured mesh and domain decomposition, as in that section, we partition each ξ into subsets related to the sets of nodes of the subdomain vertices, edges, and faces. With $\mathcal{V}$, $\mathcal{E}$, and $\mathcal{F}$ the sets of nodes of the subdomain vertices, edges, and faces, respectively, we define subcomponents ξ_i of ξ such that

$$\{\xi_i\}_{i=1}^{n_\xi} = \{\xi \cap c : c \in \mathcal{V} \cup \mathcal{E} \cup \mathcal{F} \ \wedge \ c \cap \xi \neq \emptyset\}, \tag{7.1}$$

where n_ξ is the number of subcomponents of ξ; cf. (8.2) for the analogue in case of an unstructured mesh. See Figure 2 (left) for an example in two dimensions. We next partition $K_{\xi\xi}^{\Omega_\xi}$ with respect to the subsets $\{\xi_i\}_{i=1}^{n_\xi}$ into

$$K_{\xi\xi}^{\Omega_\xi} = \left(K_{\xi_i\xi_j}^{\Omega_\xi}\right)_{i,j=1}^{n_\xi},$$

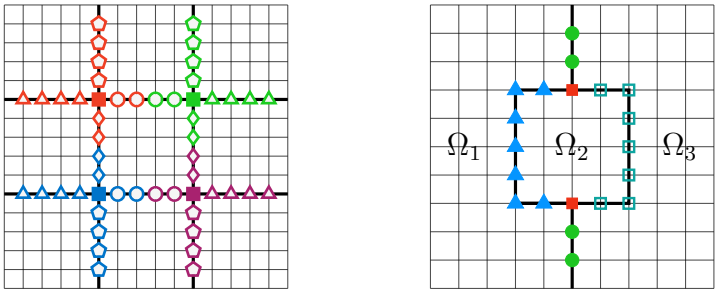

FIG. 2. *Left: Partitioning of the RGDSW interface components into the respective parts of vertices and edges as required for the right-hand side of the generalized eigenvalue problem* (7.3) *in the RAGDSW method. Each component is partitioned into* 5 *subcomponents (*4 *edges,* 1 *vertex). Right: The image shows a case in which a NEC can consist of two disjoint connected components. The interface of the domain* $\Omega = \cup_{i=1}^{3}\Omega_i$ *is indicated by thick black lines.*

and, as before, we define the Schur complement by

$$S_{\xi\xi} := K_{\xi\xi}^{\Omega_\xi} - K_{\xi R}^{\Omega_\xi}\big(K_{RR}^{\Omega_\xi}\big)^{+}K_{R\xi}^{\Omega_\xi},$$

where $\big(K_{RR}^{\Omega_\xi}\big)^{+}$ is a pseudoinverse of $K_{RR}^{\Omega_\xi}$; see Remark 9.1 and section 13. Furthermore, by removing the off-diagonal blocks from $K_{\xi\xi}^{\Omega_\xi}$, we obtain

$$\widetilde{K}_{\xi\xi} := \operatorname*{blockdiag}_{i=1,\dots,n_\xi}(K_{\xi_i\xi_i}^{\Omega_\xi}). \tag{7.2}$$

This decoupling w.r.t. the subcomponents ξ_i is essential both for the proof of Lemma 11.3 in section 11 and to obtain a robust method. Specifically, the choice of subcomponents is motivated by (11.4) in Lemma 11.3. Therein, the function Ψ is constant on ξ_i and, thus, can be moved outside of the corresponding seminorm. This would not be possible with ξ, as, in general, Ψ is not constant on ξ; as a result, the corresponding estimate would not be independent of the coefficient contrast. In fact, without the block-structure of the matrix, one can construct a mesh and coefficient function for which the algorithm fails to obtain a small condition number; see [38] for details.

We introduce a generalized eigenvalue problem, given in matrix form by

$$S_{\xi\xi}\tau_{*,\xi} = \lambda_{*,\xi}\widetilde{K}_{\xi\xi}\tau_{*,\xi}. \tag{7.3}$$

As in section 5, the eigenvalues are sorted in a nondecreasing order, and eigenvectors $\tau_{*,\xi}$ corresponding to $\lambda_{*,\xi} \leq tol_\xi$ are selected and then extended by zero to Γ^h as $\tau_{*,\Gamma}$. The coarse basis functions, i.e., the columns of Φ, corresponding to ξ are the extensions $v_{*,\xi} := H_\Gamma \tau_{*,\Gamma}$.

Remark 7.1. If $tol_\xi = 0$ for all $\xi \in \mathcal{P}$, the RAGDSW coarse space contains only the coarse functions associated with the null space of the Schur complement $S_{\xi\xi}$. The latter is identical to the null space of K^{Ω_ξ} restricted to ξ. Thus, in this case, RAGDSW reduces to RGDSW, and we have

$$V_{\mathrm{RGDSW}} = V_{\mathrm{RAGDSW}}^0 \subset V_{\mathrm{RAGDSW}}^{tol(\mathcal{P})}.$$

See also Remark 5.1.

8. Interface partitioning for RAGDSW on unstructured meshes. For unstructured cases, we will define the partitioning $\mathcal{P}$ using nodal equivalence classes and begin with definitions of connected components of finite element nodes and of nodal equivalence classes. The nodal equivalence classes are generalizations of subdomain vertices, edges, and faces and are defined using the set of adjacent subdomains. For example, the nodes of a subdomain face are shared by the same two subdomains.

The number of adjacent subdomains is an important criterion for setting up communication patterns between subdomains. The more adjacent subdomains an interface component has, the higher the communication cost of setting up the associated generalized eigenvalue problem and the computation of an energy-minimizing extension. We note that equivalence classes have previously been used, for example, in [37, 36, 9] for similar purposes.

Two finite element nodes $x_1^h, x_2^h \in \Gamma^h$ are said to be adjacent if there exists a finite element edge or face $z \subset \Gamma$ such that $x_1^h, x_2^h \in \overline{z}$, the closure of z. A set of nodes $\gamma \subset \Gamma^h$ is said to form a connected component if, for any two nodes $x_0^h, x_s^h \in \gamma$, there exists a path $(x_0^h, \dots, x_s^h)$, $x_i^h \in \gamma$, of adjacent nodes.

For any node $x^h \in \Omega$, let

$$n(x^h) := \{i \in \{1, 2, \dots, N\} : x^h \in \overline{\Omega}_i\} \tag{8.1}$$

be the set of indices of the subdomains which have x^h in common. To partition a set of nodes $\gamma \subset \Gamma^h$, we define nodal equivalence classes (NECs) by the relation $x_1^h \sim x_2^h \Leftrightarrow n(x_1^h) = n(x_2^h)$ for nodes $x_1^h, x_2^h \in \gamma$. We further partition each NEC into its connected components based on the adjacency of nodes; cf. Figure 2 (right).

By $\mathcal{N}(x^h)$, we denote the NEC of a node $x^h \in \gamma$, i.e., $x^h \in \mathcal{N}(x^h)$. If $n(x_2^h) \subsetneq n(x_1^h)$, then $\mathcal{N}(x_1^h)$ is said to be an ancestor of $\mathcal{N}(x_2^h)$, which in turn is a descendant of $\mathcal{N}(x_1^h)$. If a NEC does not have an ancestor, we call it a root.

We note that for $\gamma = \Gamma^h$, a root is a vertex in the case of cuboid subdomains; in general, we call a root a coarse node if it consists of only a single node. However, often for unstructured domain decompositions obtained, e.g., by METIS [31], a root can be a coarse edge or coarse face. An example is provided by a beam built from a union of cubes where the faces which form the interfaces between the cubes become roots; see also [9].

We now give a general description of the interface partition for RAGDSW for an unstructured mesh and domain decomposition. We will define components ξ such that each ξ contains only one root and parts of its descendants. Furthermore, we will ensure that the resulting interface partition $\mathcal{P}$ is nonoverlapping to obtain a partition $\mathcal{P}$ of connected disjoint components $\xi \in \mathcal{P}$ such that

$$\Gamma^h = \bigcup_{\xi \in \mathcal{P}} \xi.$$

Several specific constructions are possible. Relevant aspects are, e.g., obtaining components of similar size, nondegenerate components, and parallel efficiency of the construction.

For the results in this paper, we have constructed the interface partition in the following way: We initialize each component $\xi \in \mathcal{P}$ with the nodes of a root and add the remaining nodes in an iterative process.

Starting with the roots, we grow sets which will result in all the subsets $\xi \in \mathcal{P}$. In each step of an iteration, we add all nodes which are adjacent to elements of each of the current sets, which have not been previously assigned and which are descendants of the root of the set. We repeat this process until all interface nodes have been assigned to a $\xi \in \mathcal{P}$. Figure 3 depicts sample partitions for two and three dimensions.

By following this routine, we make sure that the components ξ share the same set of adjacent subdomains as the associated root, which increases parallelism. Furthermore, connected components are constructed, which usually leads to smaller coarse space dimensions. We also obtain interface components of comparable size—which increases parallelism—while still keeping the cost of construction low by adding layers of nodes in each iteration instead of single nodes. For a structured mesh with a structured domain decomposition, one could use the node coordinates instead to directly construct the interface components from section 6.

We note that for the unstructured meshes in section 14, the maximum number of degrees of freedom per eigenvalue problem is at most roughly doubled, compared to the face eigenvalue problems used in standard AGDSW. The average is increased by roughly 50%–70%, except for the problem in Figure 7: Due to the small number of subdomains, the average size of interface components is more sensitive to a change of the interface decomposition, and we obtain an increase of 155%.

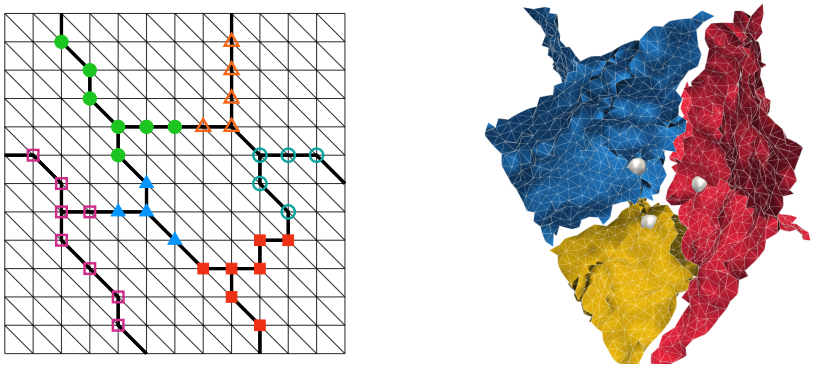

FIG. 3. *Sample partitions in two dimensions (left) and three dimensions (right) for unstructured domain decompositions. For the two-dimensional case, the interface is given by thick black lines, and the interface components $\xi \in \mathcal{P}$ are given by different markers. For the three-dimensional case, coarse nodes are indicated by white spheres; interface components are shown in different colors. For a clearer visualization, only those finite element faces are shown whose nodes are all contained in the respective interface component. Thus, gaps indicate finite element faces whose nodes are part of several interface components.*

As before, we partition each interface component into its subcomponents. Let $\mathcal{N}_{\Gamma^h}$ be the set of NECs of Γ^h, and for $\xi \in \mathcal{P}$, let

$$\mathcal{N}_\xi := \{\xi \cap c : c \in \mathcal{N}_{\Gamma^h} \ \wedge \ \xi \cap c \neq \emptyset\}. \tag{8.2}$$

Let $n_\xi := |\mathcal{N}_\xi|$ be the number of NECs of ξ, and let ξ_i, $i = 1, \dots, n_\xi$, be the resulting decomposition of ξ into $\{\xi_i\}_{i=1}^{n_\xi} = \mathcal{N}_\xi$. We then have $\xi_i \cap \xi_j = \emptyset$ $(i \neq j)$ and $\xi = \bigcup_{i=1}^{n_\xi} \xi_i$.

Remark 8.1. If our problem (2.1) satisfies a Neumann boundary condition on $\partial\Omega_N \subset \partial\Omega$, in addition to a large enough set $\partial\Omega_D = \partial\Omega \setminus \partial\Omega_N$ with a Dirichlet boundary condition to ensure unique solvability, then the construction of the RAGDSW coarse space and the proof of the condition number estimate in sections 10 and 11 will essentially be the same. Similar to standard finite element theory, the finite element nodes that lie on the Neumann boundary but not on the interface $\Gamma = \bigcup_{i \neq j} (\partial\Omega_i \cap \partial\Omega_j) \setminus \partial\Omega_D$ are treated as interior nodes since these nodes belong to only one subdomain and can be eliminated locally—just as interior nodes. For the setup of coarse functions, the same type of boundary conditions are used on the global domain boundary as for the original problem (2.1); i.e., the energy-minimizing extension (4.1) is defined such that a coarse function satisfies a homogeneous Neumann boundary condition on the nodes that lie on $\partial\Omega_N \setminus \Gamma$. This is necessary to obtain a robust method and for the proof; see (11.2) at the top of the proof of Lemma 11.2.

In the next section, we will first describe the adaptive GDSW coarse spaces in variational form. Thereafter, we will derive a condition number estimate for the preconditioned two-level additive Schwarz operator based on the coarse space introduced above. We note that the proof remains valid for quite general interface partitions $\mathcal{P}$ and is not restricted to the one of RAGDSW.

9. Variational description of adaptive GDSW-type coarse spaces. For $\xi \in \mathcal{P}$, the index set n^ξ is the set of indices of all adjacent subdomains, i.e., the union of the index sets of all nodes $x^h \in \xi$,

$$n^\xi = \bigcup_{x^h \in \xi} n(x^h). \tag{9.1}$$

As in section 5, $\overline{\Omega}_\xi$ is the closure of the union of the adjacent subdomains, i.e., $\overline{\Omega}_\xi = \bigcup_{i \in n^\xi} \overline{\Omega}_i$.

Let G be any set of finite element nodes that includes ξ. We associate finite element spaces $X^h(\xi)$ and $X^h(G)$ with these sets. Thus, let $\hat{G}$ be the interior of the union of the supports of all basis functions associated with G, define $\hat{\xi}$ similarly, and let $X^h(G) := V^h(\hat{G})$ and $X^h(\xi) := V^h(\hat{\xi})$. We can now define an extension-by-zero operator from ξ to G:

$$
\begin{aligned}
&z_{\xi \to G} : X^h(\xi) \to X^h(G) \\
&\qquad v \mapsto z_{\xi \to G}(v) := \begin{cases} v(x^h) & \forall x^h \in \xi, \\ 0 & \forall x^h \in G \setminus \xi. \end{cases}
\end{aligned} \tag{9.2}
$$

By $\mathcal{H}_{\xi \to \Omega_\xi}(\cdot)$, we denote a possibly nonunique (cf. Remark 9.1) energy-minimizing extension w.r.t. $a_{\Omega_\xi}(\cdot,\cdot)$ from ξ to $\overline{\Omega}_\xi$: Let $V^h_{0,\xi}(\Omega_\xi) := \{w \in V^h(\Omega_\xi) : w(x^h) = 0 \ \forall x^h \in \xi\}$. Then for $\tau_\xi \in X^h(\xi)$, an extension $v_\xi := \mathcal{H}_{\xi \to \Omega_\xi}(\tau_\xi) \in V^h(\Omega_\xi)$ is given by a solution of

$$
\begin{aligned}
a_{\Omega_\xi}(v_\xi, v) &= 0 && \forall v \in V^h_{0,\xi}(\Omega_\xi), \\
v_\xi(x^h) &= \tau_\xi(x^h) && \forall x^h \in \xi;
\end{aligned} \tag{9.3}
$$

cf. Figure 4. The domain of this extension operator can be extended to all $u \in V^h(\Omega)$ by working with $u|_{\hat{\xi}}$. We note that the extension is computed with a homogeneous Neumann boundary condition on $\partial\Omega_\xi$.

As in section 8, let $\{\xi_i\}_{i=1}^{n_\xi}$ be the set of all NECs of a $\xi \in \mathcal{P}$. Then $\xi_i \cap \xi_j = \emptyset$ $(i \neq j)$, and $\xi = \bigcup_{i=1}^{n_\xi} \xi_i$ holds. We define the symmetric, positive definite bilinear form

$$
c_\xi(u,v) := \sum_{i=1}^{n_\xi} c_{\xi_i}(u,v) \quad \forall u, v \in X^h(\xi), \tag{9.4}
$$

with

$$
c_{\xi_i}(u,v) := a_{\Omega_{\xi_i}}\left(z_{\xi_i \to \Omega_{\xi_i}}(u), z_{\xi_i \to \Omega_{\xi_i}}(v)\right) \quad \forall u, v \in X^h(\xi_i). \tag{9.5}
$$

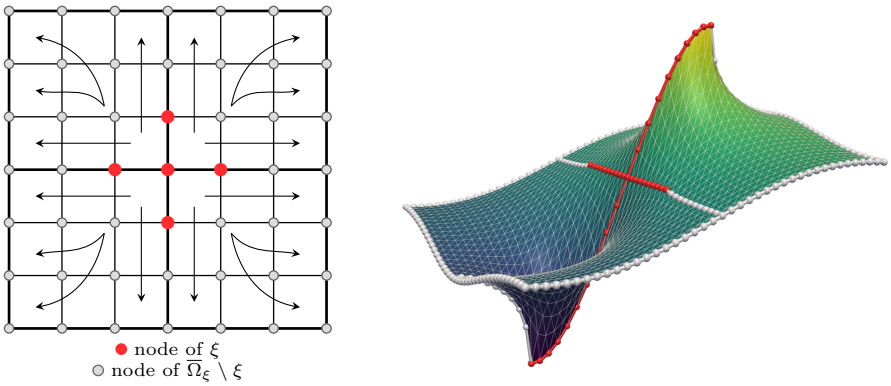

FIG. 4. *Graphical representation in two dimensions of the energy-minimizing extension* (9.3) *from $\xi \in \mathcal{P}$ to $\overline{\Omega}_\xi$ (left) and sample energy-minimizing extension for the diffusion equation (right) in which the RAGDSW interface component ξ is highlighted in red and the remaining interface nodes in light gray.*

We extend $c_{\xi_i}(u,v)$ to all of $V^h(\Omega)\times V^h(\Omega)$ by working with $u|_{\hat{\xi}_i}$ and $v|_{\hat{\xi}_i}$. The corresponding norm is defined by

$$\|u\|^2_{c_\xi} := c_\xi(u,u) \quad \forall u \in X^h(\xi). \tag{9.6}$$

We define the following generalized eigenvalue problem on $\xi\in\mathcal{P}$, which corresponds to the variational formulation of (7.3): Find $\tau_{*,\xi}\in X^h(\xi)$ such that

$$a_{\Omega_\xi}\left(\mathcal{H}_{\xi\to\Omega_\xi}(\tau_{*,\xi}),\mathcal{H}_{\xi\to\Omega_\xi}(\theta)\right) = \lambda_{*,\xi}c_\xi(\tau_{*,\xi},\theta) \quad \forall\theta\in X^h(\xi). \tag{9.7}$$

The eigenvalues are again sorted in nondescending order, i.e., $0=\lambda_{1,\xi}\le\lambda_{2,\xi}\le\ldots\le\lambda_{m,\xi}$, and the eigenmodes accordingly, where $m=\dim\left(X^h(\xi)\right)$. Furthermore, let the eigenmodes $\tau_{*,\xi}$ satisfy $c_\xi(\tau_{k,\xi},\tau_{j,\xi})=\delta_{kj}$, where δ_{kj} is the Kronecker delta symbol. We select all eigenmodes $\tau_{*,\xi}$ where the eigenvalues are below a certain threshold, i.e., $\lambda_{*,\xi}\le tol_\xi$. Then the coarse basis functions corresponding to ξ are the extensions

$$v_{*,\xi} := \mathcal{H}_{\Gamma\to\Omega}(\tau_{*,\Gamma})\in\mathring{V}^h(\Omega), \quad \tau_{*,\Gamma} := z_{\xi\to\Gamma}(\tau_{*,\xi}) \tag{9.8}$$

of the selected $\tau_{*,\xi}$, where $v_{*,\xi}=\mathcal{H}_{\Gamma\to\Omega}(\tau_{*,\Gamma})$ is given by the solution $v_{*,\xi}\in\mathring{V}^h(\Omega)$ that satisfies

$$\begin{aligned} a_{\Omega_l}(v_{*,\xi},w) &= 0 \qquad\qquad \forall w\in V^h(\Omega_l)\cap\left(H^1_0(\Omega_l)\right)^3, l=1,\ldots,N,\\ v_{*,\xi}(x^h) &= \tau_{*,\Gamma}(x^h) \quad \forall x^h\in\Gamma^h. \end{aligned} \tag{9.9}$$

We note that, contrary to (9.7), $v_{*,\xi}$ vanishes on $\partial\Omega_\xi$ since $\tau_{*,\Gamma}=z_{\xi\to\Gamma}(\tau_{*,\xi})$ and since $v_{*,\xi}=\mathcal{H}_{\Gamma\to\Omega}(\tau_{*,\Gamma})\in\mathring{V}^h(\Omega)$. Therefore, (9.9) has a unique solution.

For a general interface partition $\mathcal{P}$, we define the adaptive GDSW coarse space as

$$V_{\mathcal{P}} := \bigoplus_{\xi\in\mathcal{P}} \operatorname{span}\left\{v_{k,\xi} : \lambda_{k,\xi}\le tol_\xi\right\}. \tag{9.10}$$

We note that the standard AGDSW coarse space (see [23]) is based on the partition

$$\mathcal{P} := \mathcal{F}\cup\mathcal{E}\cup\mathcal{V}.$$

Since the sets of nodes for the vertices, edges, and faces are NECs, we then have

$$c_\xi(u,v) = a_{\Omega_\xi}\left(z_{\xi\to\Omega_\xi}(u), z_{\xi\to\Omega_\xi}(v)\right)$$

if ξ is associated with a vertex, an edge, or a face.

Remark 9.1. For the diffusion case, the energy-minimizing extension fulfilling (9.3) has a unique solution. If an interface component ξ is a straight edge or a vertex, then 1 or 3 linearized rotations, respectively, are in the null space of (9.3) for linear elasticity. However, as all solutions of (9.3) have the same energy, the choice of the particular solution does not influence the solution of the generalized eigenvalue problem (9.7): Let $v_{*,\xi}=\mathcal{H}_{\xi\to\Omega_\xi}(\tau_{*,\xi})$ be a solution of (9.3). Then all solutions of (9.3) are given by $v_{*,\xi}+r$, where r is a solution of (9.3) given that $r|_\xi=0$; for linear elasticity, r is a rigid body mode. Since $r\in V^h_{0,\xi}(\Omega_\xi)$, we have $a_{\Omega_\xi}\left(r,\mathcal{H}_{\xi\to\Omega_\xi}(\theta)\right)=0$ by the definition of $\mathcal{H}_{\xi\to\Omega_\xi}(\theta)$. Therefore, we obtain the equality

$$a_{\Omega_\xi}\left(v_{*,\xi}+r,\mathcal{H}_{\xi\to\Omega_\xi}(\theta)\right) = a_{\Omega_\xi}\left(v_{*,\xi},\mathcal{H}_{\xi\to\Omega_\xi}(\theta)\right) \quad \forall\theta\in X^h(\xi).$$

As a consequence, any operator defined by (9.3) yields the same generalized eigenvalue problem (9.7). In section 13, we will indicate how to find the solution of (9.3) if it is not unique.

Remark 9.2. We note that the left-hand side of eigenvalue problem (9.7) is singular and that its kernel contains the constant functions for the scalar diffusion case and the rigid body modes for linear elasticity. Therefore, the null space has a dimension of 1 for the scalar diffusion problem and at least 3 for linear elasticity. For a vertex (i.e., $\xi = v \in \mathcal{V}$), the problem has only one (scalar diffusion) and three (linear elasticity) degrees of freedom. Thus, in the latter case, the solution is given by the vertex basis functions of the GDSW coarse space, i.e., the three translations in case of linear elasticity; cf. [23] and [7].

10. Spectral projections. We will now consider the projections

$$\Pi_{\mathcal{P}} w := \sum_{\xi \in \mathcal{P}} \Pi_\xi w, \qquad \Pi_\xi w := \sum_{\lambda_{k,\xi} \leq tol_\xi} c_\xi(w, v_{k,\xi}) v_{k,\xi} \tag{10.1}$$

onto the space $V_{\mathcal{P}}$. Here, $v_{k,\xi}$ are the energy-minimizing extensions of the eigenfunctions determined by (9.8) and $\lambda_{k,\xi}$ the corresponding eigenvalues from (9.7). For $\xi \in \mathcal{P}$, let $d_\xi \colon X^h(\xi) \times X^h(\xi) \to \mathbb{R}$ be the symmetric, positive semidefinite bilinear form

$$d_\xi(\cdot,\cdot) := a_{\Omega_\xi}\left(\mathcal{H}_{\xi\to\Omega_\xi}(\cdot), \mathcal{H}_{\xi\to\Omega_\xi}(\cdot)\right), \tag{10.2}$$

which is used on the left-hand side of the generalized eigenvalue problem (9.7). $d_\xi(\cdot,\cdot)$ can also be extended to $V^h(\Omega) \times V^h(\Omega)$ given that we have extended the domain of $\mathcal{H}_{\xi\to\Omega_\xi}$.

For any union $B \subset \overline{\Omega}$ of finite elements $T \in \tau_h$, let

$$|v|^2_{a(B)} := a_B(v,v) \quad \forall v \in V^h(\Omega). \tag{10.3}$$

We find that

$$|v|^2_{d_\xi} := d_\xi(v,v) = |\mathcal{H}_{\xi\to\Omega_\xi}(v)|^2_{a(\Omega_\xi)} \leq |v|^2_{a(\Omega_\xi)} \quad \forall\, v \in V^h(\Omega) \tag{10.4}$$

due to the energy-minimizing property of the extension operator.

Using standard arguments of spectral theory, we obtain two important properties of the projection Π_ξ, required for the proof of the condition number estimate in section 11; cf., e.g., [12, section 2], [47, Lemma 2.11], [22, Lemma 4.1], and [23, Lemma 5.3].

LEMMA 10.1. *Let the eigenpairs* $\{(\tau_{k,\xi}, \lambda_{k,\xi})\}_{k=1}^{\dim(X^h(\xi))}$ *from* (9.7) *be chosen such that* $c_\xi(\tau_{k,\xi}, \tau_{j,\xi}) = \delta_{kj}$ *and such that the eigenpairs are sorted in nondescending order w.r.t. the eigenvalues. Then the operator* Π_ξ *defines a projection which is orthogonal with respect to the bilinear form* $d_\xi(\cdot,\cdot)$*, and therefore*

$$|u|^2_{d_\xi} = |\Pi_\xi u|^2_{d_\xi} + |u - \Pi_\xi u|^2_{d_\xi} \quad \forall u \in X^h(\xi).$$

In addition, we have, from spectral theory,

$$\|u - \Pi_\xi u\|^2_{c_\xi} \leq \frac{1}{tol_\xi} |u - \Pi_\xi u|^2_{d_\xi}.$$

The following lemma follows directly from Lemma 10.1; cf. [23, Lemma 5.4].

LEMMA 10.2. *For* $\xi \in \mathcal{P}$ *and* $u \in V^h(\Omega)$*, it holds that*

$$\|u - \Pi_\xi u\|^2_{c_\xi} \leq \frac{1}{tol_\xi} \sum_{k \in n^\xi} |u|^2_{a(\Omega_k)}.$$

Proof. We have

$$\|u-\Pi_\xi u\|_{c_\xi}^2 \overset{Lemma\ 10.1}{\leq} \frac{1}{tol_\xi}|u-\Pi_\xi u|_{d_\xi}^2 \leq \frac{1}{tol_\xi}|u|_{d_\xi}^2 \overset{(10.4)}{\leq} \frac{1}{tol_\xi}|u|_{a(\Omega_\xi)}^2 = \frac{1}{tol_\xi}\sum_{k\in n^\xi}|u|_{a(\Omega_k)}^2. \qquad \square$$

11. Convergence analysis. To prove a condition number estimate, we will prove the existence of a stable decomposition; cf. [49, Chapter 2]. We therefore define the coarse interpolation $I_0 := \Pi_{\mathcal{P}}$ as the projection onto the coarse space $V_0 := V_{\mathcal{P}}$; cf. (9.10) and (10.1). Thus, the coarse component of the stable decomposition is defined as

$$u_0 := I_0 u := \Pi_{\mathcal{P}} u.$$

LEMMA 11.1. *For $\xi \in \mathcal{P}$ and $u \in V^h(\Omega)$, we have (cf.* [23, *Lemma* 6.2]*)*

$$\|u-u_0\|_{c_\xi}^2 = c_\xi(u-u_0,u-u_0) \leq \frac{1}{tol_\xi}\sum_{k\in n^\xi}|u|_{a(\Omega_k)}^2.$$

Proof. We have

$$\begin{aligned}\|u-u_0\|_{c_\xi}^2 &= \sum_{i=1}^{n_\xi}|z_{\xi_i\to\Omega_{\xi_i}}(u-\Pi_{\mathcal{P}}u)|_{a(\Omega_{\xi_i})}^2 \\ &= \sum_{i=1}^{n_\xi}|z_{\xi_i\to\Omega_{\xi_i}}(u-\Pi_\xi u)|_{a(\Omega_{\xi_i})}^2 \\ &= \|u-\Pi_\xi u\|_{c_\xi}^2 \\ &\overset{Lemma\ 10.2}{\leq} \frac{1}{tol_\xi}\sum_{k\in n^\xi}|u|_{a(\Omega_k)}^2. \end{aligned} \qquad \square$$

Next, we derive an estimate for the energy of the coarse component; cf. [23, Lemma 6.3].

LEMMA 11.2. *It holds that*

$$|u_0|_{a(\Omega)}^2 \leq 2|u|_{a(\Omega)}^2 + \frac{2C_\tau}{tol_{\mathcal{P}}}\sum_{\xi\in\mathcal{P}}\sum_{k\in n^\xi}|u|_{a(\Omega_k)}^2 \leq 2\left(1+\frac{C_\tau N^\xi}{tol_{\mathcal{P}}}\right)|u|_{a(\Omega)}^2,$$

where C_τ is the maximum number of vertices of any element $T \in \tau_h(\Omega)$, and

$$N^\xi := \max_{1\leq i\leq N}|\mathcal{P}(\Omega_i)|, \quad \mathcal{P}(\Omega_i) := \{\xi\in\mathcal{P}\colon \xi\cap\overline{\Omega}_i \neq \emptyset\} \tag{11.1}$$

is the maximum number of interface components $\xi \in \mathcal{P}$ of any subdomain, and $tol_{\mathcal{P}} := \min_{\xi\in\mathcal{P}} tol_\xi$.

Proof. We can use the fact that u_0 is energy-minimizing w.r.t. $|\cdot|_{a(\Omega_i)}$ for each subdomain Ω_i, i.e., $u_0 = \mathcal{H}_{\Gamma\to\Omega}(u_0)$, and obtain (cf. [16, Lemma 4.1])

$$\begin{aligned}|u_0|_{a(\Omega)}^2 &\leq 2|\mathcal{H}_{\Gamma\to\Omega}(u)|_{a(\Omega)}^2 + 2|\mathcal{H}_{\Gamma\to\Omega}(u-u_0)|_{a(\Omega)}^2 \\ &\leq 2|u|_{a(\Omega)}^2 + 2|z_{\Gamma\to\Omega}(u-u_0)|_{a(\Omega)}^2. \end{aligned} \tag{11.2}$$

Let

$$\mathcal{N}_{ec,\mathcal{P}} := \bigcup_{\xi\in\mathcal{P}} \{\xi_i, i = 1, \dots, n_\xi\} \tag{11.3}$$

be the set of interface components ξ_i of $\xi \in \mathcal{P}$ partitioned according to their nodal equivalence classes ξ_i, $i = 1, \dots, n_\xi$. Then $\xi_i \cap \xi_j = \emptyset$ for $i \neq j$, $\bigcup_{\xi_i\in\mathcal{N}_{ec,\mathcal{P}}} \xi_i = \Gamma^h$, and

$$\begin{aligned} |z_{\Gamma\to\Omega}(u - u_0)|^2_{a(\Omega)} &= \Big| \sum_{\xi_i\in\mathcal{N}_{ec,\mathcal{P}}} z_{\xi_i\to\Omega}(u - u_0)\Big|^2_{a(\Omega)} \\ &= \sum_{T\in\tau_h(\Omega)} \Big| \sum_{\xi_i\in\mathcal{N}_{ec,\mathcal{P}}} z_{\xi_i\to\Omega}(u - u_0)\Big|^2_{a(T)}. \end{aligned}$$

There can be at most C_τ NECs ξ_i that are nonzero in any element T. Thus, we have, using the Cauchy–Schwarz inequality,

$$\begin{aligned} \sum_{T\in\tau_h(\Omega)} \Big| \sum_{\xi_i\in\mathcal{N}_{ec,\mathcal{P}}} z_{\xi_i\to\Omega}(u - u_0)\Big|^2_{a(T)} &\le \sum_{T\in\tau_h(\Omega)} C_\tau \sum_{\xi_i\in\mathcal{N}_{ec,\mathcal{P}}} |z_{\xi_i\to\Omega}(u - u_0)|^2_{a(T)} \\ &= C_\tau \sum_{\xi_i\in\mathcal{N}_{ec,\mathcal{P}}} |z_{\xi_i\to\Omega}(u - u_0)|^2_{a(\Omega_{\xi_i})} \\ &= C_\tau \sum_{\xi\in\mathcal{P}} \|u - u_0\|^2_{c_\xi} \\ &\le \frac{C_\tau}{tol_{\mathcal{P}}} \sum_{\xi\in\mathcal{P}} \sum_{k\in n^\xi} |u|^2_{a(\Omega_k)}, \end{aligned}$$

where in the last step we have used Lemma 11.1. Thus,

$$|u_0|^2_{a(\Omega)} \le 2|u|^2_{a(\Omega)} + 2\frac{C_\tau}{tol_{\mathcal{P}}} \sum_{\xi\in\mathcal{P}} \sum_{k\in n^\xi} |u|^2_{a(\Omega_k)} \le 2\left(1 + \frac{C_\tau N^\xi}{tol_{\mathcal{P}}}\right) |u|^2_{a(\Omega)}. \qquad \square$$

In Lemma 11.4, we will derive estimates based on the product of $u - u_0$ and a partition of unity function θ_i associated with each subdomain. We employ an overlapping decomposition $\{\tilde{\Omega}_i\}_{i=1}^N$ with overlap h by extending the nonoverlapping decomposition $\{\Omega_i\}_{i=1}^N$ by one layer of finite elements. The estimates are carried out separately on $\tilde{\Omega}_i \setminus \Omega_i$ and Ω_i: the former locally and the latter globally. The following Lemma 11.3 covers both cases; cf. [23, Lemma 6.4].

The condition number estimate in Theorem 11.5 does not reflect the fact that the rate of convergence of the algorithm often improves if the overlap is increased. The reason that the estimate does not depend on the size of the overlap is that—instead of the overlapping decomposition $\{\Omega'_i\}_{i=1}^N$ in which an overlap with one or more layers of finite elements is used for the first level of the preconditioner—the decomposition $\{\tilde{\Omega}_i\}_{i=1}^N$ with overlap h is used in the proof for technical reasons. However, this does not restrict the use of a larger overlap in the algorithmic formulation of the first level of the preconditioner.

In Table 2, a few numerical results for different sizes of the overlap are shown. As expected, we can observe an initial decrease of the number of iterations but an increase if the overlap is too large. Let us note that the condition number bound proved in Theorem 11.5 contains the constant $\hat{N}_C$, which is an upper bound for the number of overlapping subdomains any finite element point can belong to. Thus, the condition number may also grow if the overlap is increased.

TABLE 2

Results for RAGDSW–S (see section 12), two different tolerances for the selection of eigenfunctions, the coefficient function E from Figure 7 (see also Table 4), and resulting iteration counts and condition numbers for different sizes of the overlap δ; here, δ = kh means k layers of finite elements. For more details, see the caption of Table 4.

		$\delta = 1h$	$\delta = 2h$	$\delta = 3h$	$\delta = 4h$	$\delta = 5h$
$tol = 0.01$	it.	125	100	94	94	96
	κ	152.1	87.6	76.4	73.5	72.9
$tol = 0.0001$	it.	349	308	292	292	320
	κ	4 263.3	4 436.6	4 646.9	5 248.6	5 842.7

LEMMA 11.3. *Let $l \in \{0, 1, \dots, N\}$ and $B = \tilde{\Omega}_l \setminus \Omega_l$ if $l > 0$ and $B = \Omega_0 := \Omega$ for $l = 0$. Furthermore, let $\Psi : \overline{B} \to \mathbb{R}$ be a scalar-valued finite element function such that $\Psi|_{\xi_i}$ is constant on $\xi_i \in \mathcal{N}_{ec,\mathcal{P}}$, $\xi_i \subset \overline{B}$, i.e., $\Psi(x^h) = C_i$ for all $x^h \in \xi_i$, and assume that $0 \le \Psi \le 1$ and $\Psi(x^h) = 0$ for $x^h \notin \Gamma^h \cap \overline{B}$. Then*

$$|I^h(\Psi \cdot (u - u_0))|^2_{a(B)} \le \frac{C_\tau}{tol_{\mathcal{P}}} \sum_{\xi \in \mathcal{P}(\Omega_l)} \sum_{k \in n^\xi} |u|^2_{a(\Omega_k)},$$

where $I^h(\cdot)$ is the pointwise interpolation operator of the finite element space $V^h(\Omega)$.

Proof. We define the set $\mathcal{N}_{ec,\mathcal{P}}(\Omega_l) := \{\xi_j \in \mathcal{N}_{ec,\mathcal{P}} : \xi_j \cap \overline{\Omega}_l \neq \emptyset\}$ of NECs that are part of or touch Ω_l. Given that $\mathcal{P}(\Omega_0) = \mathcal{P}$, we have $\mathcal{N}_{ec,\mathcal{P}}(\Omega_0) = \mathcal{N}_{ec,\mathcal{P}}$. Since $z_{\xi_i \to B}(\cdot)$ acts as an identity operator on ξ_i, we have with $w := u - u_0$

$$\begin{aligned} |I^h(\Psi \cdot w)|^2_{a(B)} &= \Big| \sum_{\xi_i \in \mathcal{N}_{ec,\mathcal{P}}(\Omega_l)} z_{\xi_i \to B}(I^h(\Psi \cdot w)) \Big|^2_{a(B)} \\ &= \sum_{T \in \tau_h(B)} \Big| \sum_{\xi_i \in \mathcal{N}_{ec,\mathcal{P}}(\Omega_l)} z_{\xi_i \to B}(I^h(\Psi \cdot w)) \Big|^2_{a(T)}. \end{aligned}$$

There can be at most C_τ NECs ξ_i that are nonzero in any element T. Thus, we have, using the Cauchy–Schwarz inequality,

$$\Big| \sum_{\xi_i \in \mathcal{N}_{ec,\mathcal{P}}(\Omega_l)} z_{\xi_i \to B}(I^h(\Psi \cdot w)) \Big|^2_{a(T)} \le C_\tau \sum_{\xi_i \in \mathcal{N}_{ec,\mathcal{P}}(\Omega_l)} \Big| z_{\xi_i \to B}(I^h(\Psi \cdot w)) \Big|^2_{a(T)}$$

and consequently

$$|I^h(\Psi \cdot w)|^2_{a(B)} \le C_\tau \sum_{\xi_i \in \mathcal{N}_{ec,\mathcal{P}}(\Omega_l)} \Big| z_{\xi_i \to \Omega_{\xi_i}}(I^h(\Psi \cdot w)) \Big|^2_{a(\Omega_{\xi_i})}.$$

Since $0 \le \Psi \le 1$ is constant on a NEC $\xi_i \in \mathcal{N}_{ec,\mathcal{P}}(\Omega_l)$, we have

$$\begin{aligned} \sum_{\xi_i \in \mathcal{N}_{ec,\mathcal{P}}(\Omega_l)} \Big| z_{\xi_i \to \Omega_{\xi_i}}(I^h(\Psi \cdot w)) \Big|^2_{a(\Omega_{\xi_i})} &= \sum_{\xi_i \in \mathcal{N}_{ec,\mathcal{P}}(\Omega_l)} \big(\Psi|_{\xi_i}\big)^2 \Big| z_{\xi_i \to \Omega_{\xi_i}}(w) \Big|^2_{a(\Omega_{\xi_i})} \\ &\le \sum_{\xi_i \in \mathcal{N}_{ec,\mathcal{P}}(\Omega_l)} \Big| z_{\xi_i \to \Omega_{\xi_i}}(w) \Big|^2_{a(\Omega_{\xi_i})} \\ &\le \sum_{\xi \in \mathcal{P}(\Omega_l)} \sum_{i=1}^{n_\xi} \Big| z_{\xi_i \to \Omega_{\xi_i}}(w) \Big|^2_{a(\Omega_{\xi_i})} \\ &= \sum_{\xi \in \mathcal{P}(\Omega_l)} c_\xi(w, w). \end{aligned} \tag{11.4}$$

Using Lemma 11.1, we obtain

$$C_\tau \sum_{\xi\in\mathcal{P}(\Omega_l)} c_\xi(u-u_0,u-u_0) \le \frac{C_\tau}{tol_{\mathcal{P}}} \sum_{\xi\in\mathcal{P}(\Omega_l)} \sum_{k\in n^\xi} |u|^2_{a(\Omega_k)}.$$

Thus, in total, we have

$$|I^h(\Psi\cdot(u-u_0))|^2_{a(B)} \le \frac{C_\tau}{tol_{\mathcal{P}}} \sum_{\xi\in\mathcal{P}(\Omega_l)} \sum_{k\in n^\xi} |u|^2_{a(\Omega_k)}. \qquad \square$$

Now we are able to prove the existence of a stable decomposition.

LEMMA 11.4 (stable decomposition). *For each $u\in \mathring{V}^h(\Omega)$, there exists a decomposition $u=\sum_{i=0}^N R_i^T u_i$, $u_i\in V_i=\mathring{V}^h(\Omega_i')$, where $\Omega_0':=\Omega$ such that*

$$\sum_{i=0}^N |u_i|^2_{a(\Omega_i')} \le C_0^2 |u|^2_{a(\Omega)},$$

where $C_0^2=\left(14+(12N^\xi+\mathcal{C})\frac{C_\tau}{tol_{\mathcal{P}}}\right)$ and

$$\mathcal{C}:=\mathcal{C}\big(\{\Omega_i\}_{i=1}^N,\mathcal{P}\big):=\max_{1\le i\le N}\sum_{j=1}^N |\{\xi\in\mathcal{P}: i,j\in n^\xi\}|. \tag{11.5}$$

$\mathcal{C}$ is a measure for the $\mathcal{P}$-connectivity of the domain decomposition: Two subdomains i,j are connected if they touch the same interface component $\xi\in\mathcal{P}$, i.e., if $i,j\in n^\xi$.

Proof. On the overlapping decomposition $\{\tilde\Omega_i\}_{i=1}^N$ of width h, we consider the local components $u_i:=I^h(\theta_i\cdot(u-u_0))$ with the partition of unity $\{\theta_i\}_{i=1}^N$, $\theta_i:\overline{\Omega}\to\mathbb{R}$, which are scalar-valued finite element functions and where

$$\theta_i(x^h):=\begin{cases}\frac{1}{|n(x^h)|} & \text{if } x^h\in\overline{\Omega}_i,\\ 0 & \text{elsewhere,}\end{cases}$$

where x^h is a finite element node and $|n(x^h)|$ is the number of subdomains the node x^h is contained in.

We note that $\{\tilde\Omega_i\}_{i=1}^N$ can differ from the decomposition $\{\Omega_i'\}_{i=1}^N$ used in the first level of the preconditioner, in which an overlap with one or more layers of finite elements is used. The decomposition $\{\tilde\Omega_i\}_{i=1}^N$ is only used in the proof, and since $\tilde\Omega_i\subset\Omega_i'$, we have $u_i\in V_i$.

We define the cutoff function $\theta:\overline{\Omega}\to[0,1]$, which is a scalar-valued finite element function such that

$$\theta(x^h):=1-\frac{1}{|n(x^h)|} \quad \text{for any node } x^h\in\overline{\Omega}.$$

Then we have

$$\begin{aligned}
|u_i|^2_{a(\Omega_i')} &= |u_i|^2_{a(\tilde\Omega_i)} = |I^h(\theta_i(u-u_0))|^2_{a(\tilde\Omega_i)}\\
&= |I^h(\theta_i(u-u_0))|^2_{a(\Omega_i)} + |I^h(\theta_i(u-u_0))|^2_{a(\tilde\Omega_i\setminus\Omega_i)}\\
&\le 2|I^h((1-\theta_i)(u-u_0))|^2_{a(\Omega_i)} + 2|u-u_0|^2_{a(\Omega_i)} + |I^h(\theta_i(u-u_0))|^2_{a(\tilde\Omega_i\setminus\Omega_i)}\\
&\le 2|I^h(\theta(u-u_0))|^2_{a(\Omega_i)} + 4|u|^2_{a(\Omega_i)} + 4|u_0|^2_{a(\Omega_i)} + |I^h(\theta_i(u-u_0))|^2_{a(\tilde\Omega_i\setminus\Omega_i)}.
\end{aligned}$$

As θ satisfies the assumptions of Lemma 11.3, it follows that

$$\begin{aligned}\sum_{i=1}^{N} 2|I^h(\theta(u-u_0))|^2_{a(\Omega_i)} &= 2|I^h(\theta(u-u_0))|^2_{a(\Omega)} \\ &\leq 2\frac{C_\tau}{tol_{\mathcal{P}}} \sum_{\xi\in\mathcal{P}} \sum_{k\in n^\xi} |u|^2_{a(\Omega_k)} \\ &\leq 2\frac{C_\tau N^\xi}{tol_{\mathcal{P}}} |u|^2_{a(\Omega)}. \end{aligned} \tag{11.6}$$

Similarly, we have

$$\sum_{i=1}^{N} |I^h(\theta_i(u-u_0))|^2_{a(\tilde{\Omega}_i\setminus\Omega_i)} \leq \frac{C_\tau}{tol_{\mathcal{P}}} \sum_{i=1}^{N} \sum_{\xi\in\mathcal{P}(\Omega_i)} \sum_{k\in n^\xi} |u|^2_{a(\Omega_k)} \leq \mathcal{C}\frac{C_\tau}{tol_{\mathcal{P}}} |u|^2_{a(\Omega)}. \tag{11.7}$$

Thus, using (11.6), (11.7), and Lemma 11.2, we obtain

$$\begin{aligned}\sum_{i=0}^{N} |u_i|^2_{a(\Omega_i')} &= |u_0|^2_{a(\Omega)} + \sum_{i=1}^{N} |u_i|^2_{a(\tilde{\Omega}_i)} \\ &\leq 5|u_0|^2_{a(\Omega)} + 4|u|^2_{a(\Omega)} + 2\frac{C_\tau N^\xi}{tol_{\mathcal{P}}} |u|^2_{a(\Omega)} + \frac{C_\tau \mathcal{C}}{tol_{\mathcal{P}}} |u|^2_{a(\Omega)} \\ &\leq 5\cdot 2\left(1 + \frac{C_\tau N^\xi}{tol_{\mathcal{P}}}\right) |u|^2_{a(\Omega)} + \left(4 + (2N^\xi + \mathcal{C})\frac{C_\tau}{tol_{\mathcal{P}}}\right) |u|^2_{a(\Omega)} \\ &= \left(14 + (12N^\xi + \mathcal{C})\frac{C_\tau}{tol_{\mathcal{P}}}\right) |u|^2_{a(\Omega)}. \end{aligned}$$

∎

From Lemma 11.4, we directly obtain a condition number estimate for the preconditioned system.

THEOREM 11.5. *The condition number of the RAGDSW two-level Schwarz operator in three dimensions is bounded by*

$$\kappa\left(M^{-1}_{\mathrm{RAGDSW}} K\right) \leq \left(14 + (12N^\xi + \mathcal{C})\frac{C_\tau}{tol_{\mathcal{P}}}\right)\left(\hat{N}_c + 1\right),$$

where $\hat{N}_c$ is an upper bound for the number of overlapping subdomains $\{\Omega_i'\}_{i=1}^N$ any point $x^h \in \Omega$ can belong to. All constants are independent of H, h, and the contrast of Young's modulus E.

Proof. Since we use exact local solvers, we directly obtain

$$\kappa\left(M^{-1}_{\mathrm{RAGDSW}} K\right) \leq C_0^2\left(\hat{N}_c + 1\right),$$

where C_0^2 is the constant of the stable decomposition; cf. [49, Lemma 3.11] and the follow-up discussion and the proof of [11, Theorem 4.1]. We obtain the final estimate using Lemma 11.4. ∎

12. A variant using local Neumann problems. We will now describe a technique that can significantly speed up the algorithm in a parallel setting and greatly facilitate its implementation; cf. [23, section 7.2] and see also [38] for more details.

We first consider the case of an interface component which is a coarse face f. The energy-minimizing extension used in the generalized eigenvalue problem (9.7) is only

weakly coupled between the two subdomains via the nodes adjacent to the face; i.e., $\left(\Gamma^h \cap \overline{\Omega}_i \cap \overline{\Omega}_j\right) \setminus f$ contains relatively few nodes on certain coarse edges and at certain coarse nodes. Instead of computing this coupled extension $\mathcal{H}_{f\to\Omega_f}(\cdot)$ from the face f to the two adjacent subdomains as in (9.3), we can compute the extensions to each subdomain Ω_i, Ω_j separately. We expect that little information will be lost. We find that

$$a_{\Omega_\xi}\left(\mathcal{H}_{\xi\to\Omega_\xi}(\theta), \mathcal{H}_{\xi\to\Omega_\xi}(\theta)\right) \geq \sum_{k\in n^\xi} a_{\Omega_k}\left(\mathcal{H}_{\xi\to\Omega_k}(\theta), \mathcal{H}_{\xi\to\Omega_k}(\theta)\right)$$

for $\theta \in X^h(\xi)$. Since the subdomains are only weakly coupled via these adjacent nodes of the face, we expect only a small change if we replace the left-hand side of (9.7) using this alternative extension and that the dimension of the coarse space will increase only slightly.

The same technique can be applied to arbitrary interface components $\xi \in \mathcal{P}$. We might expect that the coupling will be stronger between subdomains for smaller interface components, but our numerical results in section 14 suggest that the increase in the coarse space dimension is moderate in all cases considered.

We indicate that this technique is employed by adding a trailing S to the coarse space name: $V_{\mathrm{AGDSW-S}}$ and $V_{\mathrm{RAGDSW-S}}$; cf. Figure 5. Using this modification yields the same condition number bound as in Theorem 11.5 since d_ξ^S, the modification of d_ξ, satisfies the same inequality as in (10.4):

$$|v|^2_{d_\xi^S} := d_\xi^S(v,v) := \sum_{k\in n^\xi} |\mathcal{H}_{\xi\to\Omega_k}(v)|^2_{a(\Omega_k)} \leq \sum_{k\in n^\xi} |v|^2_{a(\Omega_k)} = |v|^2_{a(\Omega_\xi)} \quad \forall v \in V^h(\Omega).$$

Let the local (nonoverlapping) stiffness matrices with a Neumann boundary for the corresponding bilinear forms $a_{\Omega_k}(\cdot,\cdot)$ be given by K^{Ω_k}. For each $\xi \in \mathcal{P}$, we partition the degrees of freedom of Ω_k into those in $\xi \cap \overline{\Omega}_k$ and the remaining ones, R. We have

$$K^{\Omega_k} = \begin{pmatrix} K^{\Omega_k}_{RR} & K^{\Omega_k}_{R\xi} \\ K^{\Omega_k}_{\xi R} & K^{\Omega_k}_{\xi\xi} \end{pmatrix}.$$

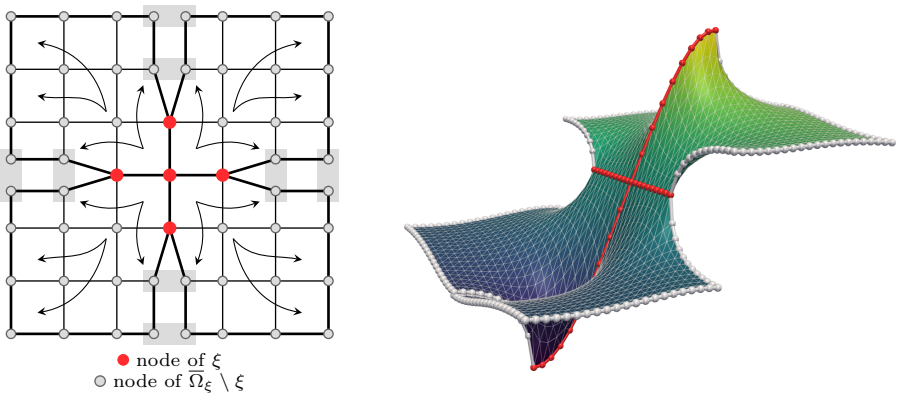

FIG. 5. *Analogue of Figure 4 for RAGDSW–S. Graphical representation in two dimensions of the energy-minimizing extensions (9.3) from $\xi \cap \overline{\Omega}_k$ to $\overline{\Omega}_k$, where $\xi \in \mathcal{P}$ and Ω_k is a subdomain adjacent to ξ (left); nodes on the interface with identical coordinates that have been torn apart to visualize multiple extension values are connected with a light gray box. Sample extension (energy-minimizing in each subdomain) for the diffusion equation (right) in which the RAGDSW interface component ξ is highlighted in red and the remaining interface nodes in light gray.*

Let R^T_{ξ,Ω_k} map the degrees of freedom of $\xi \cap \overline{\Omega}_k$ to ξ. We define

$$S^S_{\xi\xi} := \sum_{k \in n^\xi} R^T_{\xi,\Omega_k} S^k_{\xi\xi},$$

with the Schur complements

$$S^k_{\xi\xi} := K^{\Omega_k}_{\xi\xi} - K^{\Omega_k}_{\xi R} \big(K^{\Omega_k}_{RR}\big)^+ K^{\Omega_k}_{R\xi}, \quad k \in n^\xi,$$

where $\big(K^{\Omega_k}_{RR}\big)^+$ is a pseudoinverse of $K^{\Omega_k}_{RR}$; cf. Remark 9.1 and section 13. Using the definition of $\widetilde{K}_{\xi\xi}$ from (7.2), we obtain the modified generalized eigenvalue problem given in matrix form by

$$S^S_{\xi\xi} \tau_{*,\xi} = \lambda_{*,\xi} \widetilde{K}_{\xi\xi} \tau_{*,\xi}.$$

13. Remarks on the computation of the energy-minimizing extension. For an interface component $\xi \in \mathcal{P}$, the energy-minimizing extension (9.3) satisfies a homogeneous Neumann boundary condition on $\partial\Omega_\xi \setminus \xi$. Therefore, for linear elasticity, if ξ consists only of a single node or if it is given by a straight edge, then all three linearized rotations or the linearized rotation around the edge are in the null space of the problem. Thus, in such cases, the operator $\mathcal{H}_{\xi\to\Omega_\xi}(\cdot)$ defined by (9.3) is not unique; cf. Remark 9.1. Furthermore, $K^{\Omega_\xi}_{RR}$ is symmetric and only positive semidefinite.

We also note that if the variant described in section 12 is used, the matrices $K^{\Omega_k}_{RR}$ are even more likely to be singular since the extension is based on the sets $\xi \cap \overline{\Omega}_k$, $k \in n^\xi$, which are usually smaller than ξ.

In an implementation, we have several options to compute an energy-minimizing extension, i.e., to solve a system $K_{RR}x = y$, where $K_{RR} := K^{\Omega_\xi}_{RR}$ or, in case of the variant from section 12, $K_{RR} := K^{\Omega_k}_{RR}$. Theoretically, we could compute a full pseudoinverse of K_{RR}; however, this is very expensive in terms of processor time and memory. As a more efficient and algebraic alternative, a pivoted factorization can be computed such that the diagonal is rank revealing. Alternatively, we can add a small regularization term $\varepsilon\mathcal{R}$ to obtain a symmetric, positive definite problem, e.g., $\varepsilon\mathcal{R} = 10^{-13} K_{\text{diag}}$, where K_{diag} is the diagonal of K_{RR}.

We have also considered two further, geometric approaches. One approach is to remove the null space by a projection. For this, we need to determine a basis of the null space, i.e., compute the linearized rotations, which requires geometric information. This approach has another downside if we want to use a direct solver on the resulting system since transforming the system is quite expensive and the transformed system generally more dense.

A second geometric approach is less algebraic and eliminates a subset of the degrees of freedom of the matrix K_{RR} at the expense of solving a small Schur complement system using a pseudoinverse. At best, this amounts to prescribing a zero Dirichlet boundary condition on some additional degrees of freedom.

In general, we pick at least as many degrees of freedom $\tilde{D} \subset R$ as the dimension of the null space of K_{RR}. Let the remaining degrees of freedom be denoted by $\tilde{R} \subset R$. The matrix K_{RR} is partitioned by $\tilde{R}$ and $\tilde{D}$ such that

$$K_{RR} = \begin{pmatrix} K_{\tilde{R},\tilde{R}} & K_{\tilde{R},\tilde{D}} \\ K_{\tilde{D},\tilde{R}} & K_{\tilde{D},\tilde{D}} \end{pmatrix}.$$

The variables $\tilde{R}$ are then eliminated to obtain a Schur complement system

$$\begin{pmatrix} K_{\tilde{R},\tilde{R}} & K_{\tilde{R},\tilde{D}} \\ 0 & S_{\tilde{D},\tilde{D}} \end{pmatrix}, \quad S_{\tilde{D},\tilde{D}} = K_{\tilde{D},\tilde{D}} - K_{\tilde{D},\tilde{R}} K^{-1}_{\tilde{R},\tilde{R}} K_{\tilde{R},\tilde{D}}.$$

If $\tilde{D}$ was chosen properly, the submatrix $K_{\tilde{R},\tilde{R}}$ is invertible. For example, if ξ is a straight edge and $\tilde{D}$ corresponds to a node which does not lie on the same straight line as the edge (note that three degrees of freedom are associated with each node), then $K_{\tilde{R},\tilde{R}}$ is invertible. In that case, the Schur complement is well defined and has a null space of the same dimension as K_{RR}. Thus, we can solve the corresponding system using a pseudoinverse. This is much cheaper than using a pseudoinverse of K_{RR} since $S_{\tilde{D},\tilde{D}}$ is of a much smaller dimension.

If we select the degrees of freedom in $\tilde{D}$ carefully, the Schur complement will be identically zero; i.e., computing the energy-minimizing extension is no more expensive than solving a linear system with $K_{\tilde{R},\tilde{R}}$, and the cost will be comparable to that of a case with an invertible K_{RR}.

14. Numerical results. In this section, we present numerical results to compare the nonadaptive coarse spaces GDSW and RGDSW, the adaptive coarse spaces AGDSW (section 5) and RAGDSW (section 8), and their S-variants AGDSW–S and RAGDSW–S; cf. section 12. In order to compute the Schur complement and avoid the use of a pseudoinverse, we have added a regularization term with $\varepsilon = 10^{-13}$ to the respective singular matrix; cf. section 13. We remark that in [23] a short comparison of the AGDSW and the GenEO coarse space ([47]) was carried out.

We show numerical results for a discretization of problem (2.1) with a Poisson ratio $\nu = 0.4$, the right-hand side $f \equiv (1,1,1)^T$, and several coefficient functions given by different choices of the Young modulus function $E(\cdot)$. The smallest Young modulus $E_{\min} := \min_{x\in\overline{\Omega}} E(x)$ is always set to 1, and the maximum $E_{\max} := \max_{x\in\overline{\Omega}} E(x)$ is specified in the respective figure and table caption. A Dirichlet condition on the boundary of the domain Ω can reduce the number of bad eigenmodes if patches associated with large coefficients touch the Dirichlet boundary of Ω. Thus, in order to obtain a harder problem, we have constructed the coefficient functions in Figures 6–8 such that patches associated with large coefficients do not touch the Dirichlet boundary of Ω. Except for the test case of Figure 7 and Table 4, the domain Ω is the unit cube with a zero Dirichlet condition prescribed on all its boundary.

We use piecewise linear basis functions on tetrahedra and solve the resulting linear system with the preconditioned conjugate gradient (PCG) method and a relative

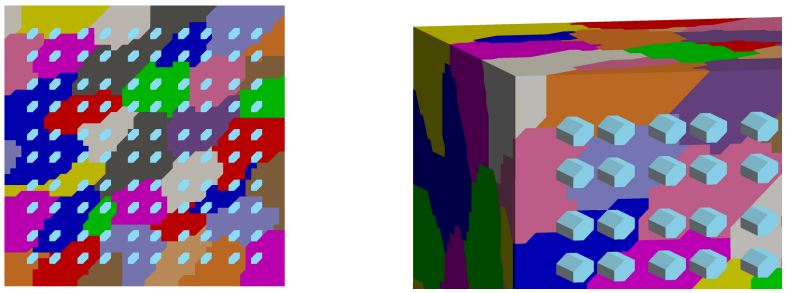

FIG. 6. *Cross section (left) of a domain decomposition of a cube and a discontinuous coefficient function E with beams of large coefficients (light blue) crossing the domain. The beams of large coefficients do not touch the domain boundary. The light blue color corresponds to a coefficient of $E_{\max} = 10^6$, and the remainder is set to $E_{\min} = 1.0$. Number of subdomains:* 125*; number of nodes:* 132 651 *(degrees of freedom:* 397 953*); average degrees of freedom per overlapping subdomain:* 6 198*; overlap: two layers of finite elements. Structured tetrahedral mesh; unstructured domain decomposition (METIS). For the corresponding results, see Table* 3*. Taken from* [23, *Figure* 8].

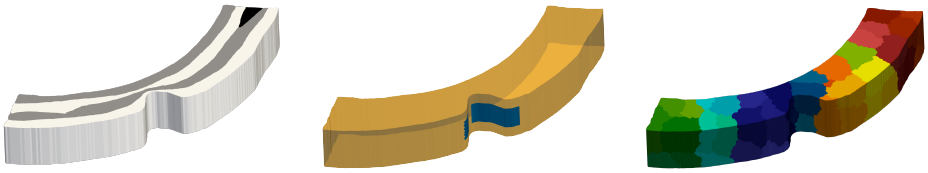

FIG. 7. *Left: Discontinuous coefficient function E with coefficient layers of $E = 10^6$ in light gray and an inclusion at the top right with $E = 10^9$ in dark gray. The remainder of the coefficient in white is set to $E_{\min} = 1.0$. Center: Boundary partition for Dirichlet (blue) and Neumann (orange) boundary. Right: Domain decomposition of 50 subdomains. Number of nodes: 56 053 (degrees of freedom: 168 159); average degrees of freedom per overlapping subdomain: 5 632.2; overlap: two layers of finite elements. Unstructured tetrahedral mesh; unstructured domain decomposition (METIS). For the corresponding results, see Table 4. Taken from* [23, *Figure* 9].

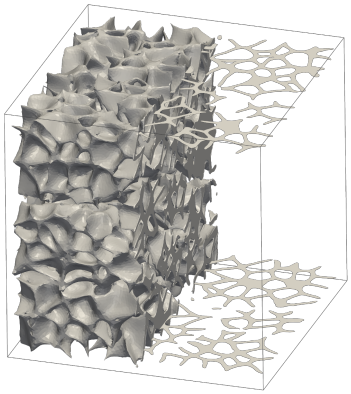

FIG. 8. *Partial visualization of an unstructured tetrahedral mesh consisting of several disconnected components of foamlike structures. On the corresponding mesh of a cube, foam corresponds to a large coefficient of $E_{\max} = 10^6$ with $E_{\min} = 1.0$ elsewhere. The large coefficient does not touch the domain boundary. Number of subdomains: 100; number of nodes: 588 958 (degrees of freedom: 1 766 874); average degrees of freedom per overlapping subdomain: 26 756.1; overlap: two layers of finite elements. Unstructured tetrahedral mesh; unstructured domain decomposition (METIS). For the corresponding results, see Table 5. Taken from* [23, *Figure* 10].

stopping criterion of $\|r^{(k)}\|_2/\|r^{(0)}\|_2 < 10^{-8}$, where $r^{(0)}$ and $r^{(k)}$ are the initial and the kth unpreconditioned residuals, respectively. The reported condition numbers are the estimates obtained after the last iteration of the PCG method using the Lanczos method [44, Chapter 6.7.3]. We partition the domain into subdomains using METIS [31]. In all experiments, we use an overlap of two layers of finite elements; see section 3 for the definition of the overlap.

The coefficient function of the first test problem is depicted in Figure 6; the corresponding results are given in Table 3. Experiments with both nonadaptive coarse spaces GDSW and RGDSW failed to converge in 2 000 iterations, clearly showing that adaptivity is required to obtain a robust preconditioner. By using the adaptive coarse spaces, we obtain acceptable condition numbers and iteration counts. The results show a significant reduction in the coarse space dimension for the RAGDSW variant compared to AGDSW. For example, ($tol = 0.05$), the dimension of $V_{\text{AGDSW}-\text{S}}$ is reduced by 43.6% by using $V_{\text{RAGDSW}-\text{S}}$. And even while GDSW does not converge in 2 000 iterations, its coarse space is 26.5% larger than that of RAGDSW–S ($tol = 0.05$).

TABLE 3

Results for the coefficient function in Figure 6: iteration counts, condition numbers, and resulting coarse space dimension for different coarse spaces. Number of subdomains: 125*; degrees of freedom:* 397 953*; overlap: two layers of finite elements; maximum coefficient* $E_{\max} = 10^6$*; relative stopping criterion* $\|r^{(k)}\|_2/\|r^{(0)}\|_2 < 10^{-8}$*. Structured tetrahedral mesh; unstructured domain decomposition (METIS).*

	Coefficient function E from Figure 6							
V_0	*tol*	it.	κ	$\dim V_0$	$(\mathcal{V}/\mathcal{P},$	$\mathcal{E}$,	$\mathcal{F}$ $)$	$\dim V_0/\text{dof}$
V_{GDSW}	–	>2 000	$3.1{\cdot}10^5$	9 996	(1 707,	4 618,	3 671)	2.51%
V_{RGDSW}	–	>2 000	$3.9{\cdot}10^5$	3 358	(3 358,	0,	0)	0.84%
V_{AGDSW}	0.100	71	41.1	14 439	(1 707,	4 943,	7 789)	3.63%
V_{AGDSW}	0.050	90	59.5	13 945	(1 707,	4 915,	7 323)	3.50%
V_{AGDSW}	0.010	132	161.1	13 763	(1 707,	4 912,	7 144)	3.46%
V_{AGDSW}	0.001	327	971.8	13 721	(1 707,	4 907,	7 107)	3.45%
$V_{\text{AGDSW-S}}$	0.100	63	28.7	14 597	(1 707,	5 020,	7 870)	3.67%
$V_{\text{AGDSW-S}}$	0.050	89	57.5	14 004	(1 707,	4 949,	7 348)	3.52%
$V_{\text{AGDSW-S}}$	0.010	134	166.0	13 767	(1 707,	4 914,	7 146)	3.46%
$V_{\text{AGDSW-S}}$	0.001	305	973.1	13 729	(1 707,	4 911,	7 111)	3.45%
V_{RAGDSW}	0.100	67	34.6	8 249	(8 249,	0,	0)	2.07%
V_{RAGDSW}	0.050	88	61.3	7 683	(7 683,	0,	0)	1.93%
V_{RAGDSW}	0.010	114	117.4	7 501	(7 501,	0,	0)	1.88%
V_{RAGDSW}	0.001	383	$1.4{\cdot}10^3$	7 401	(7 401,	0,	0)	1.86%
$V_{\text{RAGDSW-S}}$	0.100	62	32.7	8 799	(8 799,	0,	0)	2.21%
$V_{\text{RAGDSW-S}}$	0.050	79	51.4	7 903	(7 903,	0,	0)	1.99%
$V_{\text{RAGDSW-S}}$	0.010	109	104.5	7 563	(7 563,	0,	0)	1.90%
$V_{\text{RAGDSW-S}}$	0.001	268	902.7	7 525	(7 525,	0,	0)	1.89%

For the next example, we consider a problem for which we impose a Neumann boundary condition on most of the domain boundary; see Figure 7. The results in Table 4 show an even larger reduction in the coarse space dimension from AGDSW to RAGDSW compared to the previous case. We obtain a reduction of 69.4% (*tol* = 0.05). The reason for this is the larger number of interface components: Since the AGDSW space contains the GDSW space and the RAGDSW space contains the RGDSW space, a significant part of the coarse space reduction can be attributed to the smaller dimension of RGDSW compared to GDSW. This highlights the core idea behind the reduced-dimension GDSW spaces in [9]; the explanation is supported by the fact that the dimension of V_{RAGDSW} is fairly close to that of V_{RGDSW}. Therefore, since the coefficient function contains only relatively few connected large-coefficient components, only a few additional coarse basis functions are required.

We consider another realistic geometry in Figure 8 with a foamlike structure. We note that the foam is not a single connected structure but consists of several smaller disconnected foamlike structures. The results in Table 5 are similar to the previous ones. By using RAGDSW–S, we obtain a coarse space reduction of 49.9% compared to AGDSW–S (*tol* = 0.05). However, here, the dimension of $V_{\text{RAGDSW-S}}$ is more than double that of V_{RGDSW}, indicating that $V_{\text{RAGDSW-S}}$ is adaptively enriched with quite a few additional basis functions compared to V_{RGDSW}.

We conclude with averaged results for 100 random coefficient functions showing the robustness of the methods; cf. Table 6. Despite comparable number of iterations and condition numbers, the coarse space dimensions of RAGDSW(–S) are smaller by a factor of 1.6 compared to those of AGDSW(–S) (at an equal tolerance).

TABLE 4

Results for the coefficient function in Figure 7: iteration counts, condition numbers, and resulting coarse space dimension for different coarse spaces. Number of subdomains: 50; degrees of freedom: 168 159; overlap: two layers of finite elements; maximum coefficient $E_{\max} = 10^9$; relative stopping criterion $\|r^{(k)}\|_2/\|r^{(0)}\|_2 < 10^{-8}$. Unstructured tetrahedral mesh; unstructured domain decomposition (METIS). See also Table 2 for some results regarding different sizes of the overlap.

	Coefficient function E from Figure 7					
V_0	*tol*	it.	κ	$\dim V_0$	$(\mathcal{V}/\mathcal{P},\ \mathcal{E},\ \mathcal{F})$	$\dim V_0/\mathrm{dof}$
V_{GDSW}	–	1 329	$1.5{\cdot}10^7$	2 319	(291, 1 000, 1 028)	1.38%
V_{RGDSW}	–	1 549	$1.0{\cdot}10^7$	572	(572, 0, 0)	0.34%
V_{AGDSW}	0.100	60	20.2	2 732	(291, 1 058, 1 383)	1.62%
V_{AGDSW}	0.050	69	28.1	2 631	(291, 1 058, 1 282)	1.56%
V_{AGDSW}	0.010	71	28.2	2 626	(291, 1 058, 1 277)	1.56%
V_{AGDSW}	0.001	152	1 162.2	2 613	(291, 1 052, 1 270)	1.55%
$V_{\mathrm{AGDSW-S}}$	0.100	58	18.9	2 741	(291, 1 059, 1 391)	1.63%
$V_{\mathrm{AGDSW-S}}$	0.050	69	28.1	2 631	(291, 1 058, 1 282)	1.56%
$V_{\mathrm{AGDSW-S}}$	0.010	72	28.2	2 626	(291, 1 058, 1 277)	1.56%
$V_{\mathrm{AGDSW-S}}$	0.001	142	733.7	2 614	(291, 1 053, 1 270)	1.55%
V_{RAGDSW}	0.100	68	27.1	988	(988, 0, 0)	0.59%
V_{RAGDSW}	0.050	85	43.8	804	(804, 0, 0)	0.48%
V_{RAGDSW}	0.010	100	88.5	781	(781, 0, 0)	0.46%
V_{RAGDSW}	0.001	183	769.1	774	(774, 0, 0)	0.46%
$V_{\mathrm{RAGDSW-S}}$	0.100	60	20.7	1 152	(1 152, 0, 0)	0.69%
$V_{\mathrm{RAGDSW-S}}$	0.050	78	35.2	868	(868, 0, 0)	0.52%
$V_{\mathrm{RAGDSW-S}}$	0.010	100	87.6	790	(790, 0, 0)	0.47%
$V_{\mathrm{RAGDSW-S}}$	0.001	115	141.1	786	(786, 0, 0)	0.47%

TABLE 5

Results for the coefficient function in Figure 8: iteration counts, condition numbers, and resulting coarse space dimension for different coarse spaces. Number of subdomains: 100; degrees of freedom: 1 766 874; overlap: two layers of finite elements; maximum coefficient $E_{\max} = 10^6$; relative stopping criterion $\|r^{(k)}\|_2/\|r^{(0)}\|_2 < 10^{-8}$. Unstructured tetrahedral mesh; unstructured domain decomposition (METIS).

	Coefficient function E from Figure 8					
V_0	*tol*	it.	κ	$\dim V_0$	$(\mathcal{V}/\mathcal{P},\ \mathcal{E},\ \mathcal{F})$	$\dim V_0/\mathrm{dof}$
V_{GDSW}	–	1 865	$1.1{\cdot}10^6$	8 311	(1 167, 4 108, 3 036)	0.47%
V_{RGDSW}	–	1 613	$9.3{\cdot}10^5$	2 313	(2 313, 0, 0)	0.13%
V_{AGDSW}	0.10	52	21.4	12 367	(1 167, 4 358, 6 842)	0.70%
V_{AGDSW}	0.05	68	43.8	10 940	(1 167, 4 351, 5 422)	0.62%
V_{AGDSW}	0.01	167	333.4	10 304	(1 167, 4 324, 4 813)	0.58%
$V_{\mathrm{AGDSW-S}}$	0.10	50	18.7	12 539	(1 167, 4 389, 6 983)	0.71%
$V_{\mathrm{AGDSW-S}}$	0.05	63	32.2	11 005	(1 167, 4 362, 5 476)	0.62%
$V_{\mathrm{AGDSW-S}}$	0.01	147	158.1	10 320	(1 167, 4 338, 4 815)	0.58%
V_{RAGDSW}	0.10	54	22.0	6 641	(6 641, 0, 0)	0.38%
V_{RAGDSW}	0.05	80	45.2	4 868	(4 868, 0, 0)	0.28%
V_{RAGDSW}	0.01	189	280.2	4 019	(4 019, 0, 0)	0.23%
$V_{\mathrm{RAGDSW-S}}$	0.10	50	18.4	7 833	(7 833, 0, 0)	0.44%
$V_{\mathrm{RAGDSW-S}}$	0.05	69	46.1	5 519	(5 519, 0, 0)	0.31%
$V_{\mathrm{RAGDSW-S}}$	0.01	151	202.6	4 152	(4 152, 0, 0)	0.23%

Acknowledgments. We thank the Regional Computing Center of the University of Cologne (RRZK) for providing computing time on the DFG-funded High Performance Computing (HPC) system CHEOPS (DFG FKZ: INST 216/512/1FUGG) as well as support.

TABLE 6

Averaged results for 100 *random coefficient functions (average large-coefficient density:* 11.08%*): tolerance for the selection of the eigenfunctions, iteration counts, condition numbers, and resulting coarse space dimension for different coarse spaces; maximum in brackets. Number of subdomains:* 512*; number of nodes:* 452 522 *(degrees of freedom:* 1 357 566*); average degrees of freedom per overlapping subdomain:* 5 906.4*; overlap: two layers of finite elements; maximum coefficient* $E_{\max} = 10^6$*; relative stopping criterion* $\|r^{(k)}\|_2/\|r^{(0)}\|_2 < 10^{-8}$*. Unstructured tetrahedral mesh; unstructured domain decomposition (METIS).* V_{GDSW} *and* V_{RGDSW} *never converged in* 2 000 *iterations.*

	Random coefficient function E				
V_0	*tol*	it.	κ	$\dim V_0$	$\dim V_0/\mathrm{dof}$
V_{GDSW}	–	>2 000 (–)	$2.1{\cdot}10^5$ ($3.2{\cdot}10^5$)	49 862.0 (49 862)	3.7% (3.7%)
V_{RGDSW}	–	>2 000 (–)	$2.4{\cdot}10^5$ ($3.7{\cdot}10^5$)	17 778.0 (17 778)	1.3% (1.3%)
V_{AGDSW}	0.10	84.8 (93)	56.2 (80.7)	69 006.7 (69 892)	5.1% (5.1%)
V_{AGDSW}	0.05	106.3 (118)	92.1 (145.2)	66 482.5 (67 273)	4.9% (5.0%)
V_{AGDSW}	0.01	180.8 (228)	293.3 (662.9)	64 508.1 (65 235)	4.8% (4.8%)
$V_{\mathrm{AGDSW-S}}$	0.10	76.4 (84)	44.1 (54.2)	70 570.8 (71 632)	5.2% (5.3%)
$V_{\mathrm{AGDSW-S}}$	0.05	99.3 (112)	77.9 (110.7)	67 445.3 (68 360)	5.0% (5.0%)
$V_{\mathrm{AGDSW-S}}$	0.01	168.1 (195)	247.5 (448.4)	65 212.8 (66 046)	4.8% (4.9%)
V_{RAGDSW}	0.10	89.5 (100)	60.9 (82.2)	39 081.8 (39 780)	2.9% (2.9%)
V_{RAGDSW}	0.05	115.1 (129)	104.8 (152.5)	35 961.4 (36 649)	2.6% (2.7%)
V_{RAGDSW}	0.01	200.3 (232)	342.8 (523.6)	33 370.8 (34 058)	2.5% (2.5%)
$V_{\mathrm{RAGDSW-S}}$	0.10	74.9 (88)	42.8 (59.6)	44 045.9 (44 677)	3.2% (3.3%)
$V_{\mathrm{RAGDSW-S}}$	0.05	97.1 (112)	72.9 (103.5)	39 076.9 (39 730)	2.9% (2.9%)
$V_{\mathrm{RAGDSW-S}}$	0.01	167.8 (199)	244.7 (469.9)	35 399.8 (36 137)	2.6% (2.7%)

REFERENCES

[1] J. AARNES AND T. Y. HOU, *Multiscale domain decomposition methods for elliptic problems with high aspect ratios*, Acta Math. Appl. Sin. Engl. Ser., 18 (2002), pp. 63–76.

[2] P. BJØRSTAD, J. KOSTER, AND P. KRZYZANOWSKI, *Domain decomposition solvers for large scale industrial finite element problems*, in Applied Parallel Computing, New Paradigms for HPC in Industry and Academia, Lecture Notes in Computer Science 1947, Springer-Verlag, Berlin, 2001, pp. 373–383.

[3] M. BUCK, O. ILIEV, AND H. ANDRÄ, *Multiscale finite elements for linear elasticity: Oscillatory boundary conditions*, in Domain Decomposition Methods in Science and Engineering XXI, LNCSE 98, Springer-Verlag, Berlin, 2014, pp. 237–245.

[4] C. DOHRMANN AND O. B. WIDLUND, *An alternative coarse space for irregular subdomains and an overlapping Schwarz algorithm for scalar elliptic problems in the plane*, SIAM J. Numer. Anal., 50 (2012), pp. 2522–2537.

[5] C. R. DOHRMANN, A. KLAWONN, AND O. B. WIDLUND, *Domain decomposition for less regular subdomains: Overlapping Schwarz in two dimensions*, SIAM J. Numer. Anal., 46 (2008), pp. 2153–2168.

[6] C. R. DOHRMANN, A. KLAWONN, AND O. B. WIDLUND, *A family of energy minimizing coarse spaces for overlapping Schwarz preconditioners*, in Domain Decomposition Methods in Science and Engineering XVII, LNCSE 60, Springer-Verlag, Berlin, 2008, pp. 247–254.

[7] C. R. DOHRMANN AND O. B. WIDLUND, *An overlapping Schwarz algorithm for almost incompressible elasticity*, SIAM J. Numer. Anal., 47 (2009), pp. 2897–2923.

[8] C. R. DOHRMANN AND O. B. WIDLUND, *Hybrid domain decomposition algorithms for compressible and almost incompressible elasticity*, Internat. J. Numer. Methods Engrg., 82 (2010), pp. 157–183.

[9] C. R. DOHRMANN AND O. B. WIDLUND, *On the design of small coarse spaces for domain decomposition algorithms*, SIAM J. Sci. Comput., 39 (2017), pp. A1466–A1488.

[10] V. DOLEAN, F. NATAF, R. SCHEICHL, AND N. SPILLANE, *Analysis of a two-level Schwarz method with coarse spaces based on local Dirichlet-to-Neumann maps*, Comput. Methods Appl. Math., 12 (2012), pp. 391–414.

[11] M. DRYJA AND O. B. WIDLUND, *Domain decomposition algorithms with small overlap*, SIAM J. Sci.Comput., 15 (1994), pp. 604–620.

[12] Y. Efendiev, J. Galvis, R. Lazarov, and J. Willems, *Robust domain decomposition preconditioners for abstract symmetric positive definite bilinear forms*, ESAIM Math. Model. Numer. Anal., 46 (2012), pp. 1175–1199.
[13] Y. Efendiev and T. Y. Hou, *Multiscale Finite Element Methods: Theory and Applications*, Surveys and Tutorials in the Applied Mathematical Sciences, Springer-Verlag, Berlin, 2009.
[14] E. Eikeland, L. Marcinkowski, and T. Rahman, *Overlapping Schwarz methods with adaptive coarse spaces for multiscale problems in* 3*D*, Numer. Math, 142 (2019), pp. 103–128.
[15] J. Galvis and Y. Efendiev, *Domain decomposition preconditioners for multiscale flows in high contrast media: Reduced dimension coarse spaces*, Multiscale Model. Simul., 8 (2010), pp. 1621–1644.
[16] M. J. Gander, A. Loneland, and T. Rahman, *Analysis of a New Harmonically Enriched Multiscale Coarse Space for Domain Decomposition Methods*, preprint, arXiv:1512.05285, 2015.
[17] I. Graham, P. Lechner, and R. Scheichl, *Domain decomposition for multiscale PDEs*, Numer. Math., 106 (2007), pp. 589–626.
[18] A. Heinlein, *Parallel Overlapping Schwarz Preconditioners and Multiscale Discretizations with Applications to Fluid-Structure Interaction and Highly Heterogeneous Problems*, Ph.D. thesis, University of Cologne, Cologne, Germany, 2016.
[19] A. Heinlein, C. Hochmuth, and A. Klawonn, *Monolithic overlapping Schwarz domain decomposition methods with GDSW coarse spaces for incompressible fluid flow problems*, SIAM J. Sci. Comp., 41 (2019), pp. C291–C316.
[20] A. Heinlein, C. Hochmuth, and A. Klawonn, *Reduced dimension GDSW coarse spaces for monolithic Schwarz domain decomposition methods for incompressible fluid flow problems*, Internat. J. Numer. Methods Engrg., 121 (2020), pp. 1101–1119.
[21] A. Heinlein, A. Klawonn, J. Knepper, and O. Rheinbach, *An adaptive GDSW coarse space for two-level overlapping Schwarz methods in two dimensions*, in Domain Decomposition Methods in Science and Engineering XXIV, LNCSE 125, Springer-Verlag, Berlin, 2018, pp. 373–382.
[22] A. Heinlein, A. Klawonn, J. Knepper, and O. Rheinbach, *Multiscale coarse spaces for overlapping Schwarz methods based on the ACMS space in* 2*D*, ETNA, 48 (2018), pp. 156–182.
[23] A. Heinlein, A. Klawonn, J. Knepper, and O. Rheinbach, *Adaptive GDSW coarse spaces for overlapping Schwarz methods in three dimensions*, SIAM J. Sci. Comp., 41 (2019), pp. A3045–A3072.
[24] A. Heinlein, A. Klawonn, S. Rajamanickam, and O. Rheinbach, *FROSch: A fast and robust overlapping Schwarz domain decomposition preconditioner based on Xpetra in Trilinos*, in Domain Decomposition Methods in Science and Engineering XXV, LNCSE 138, Springer-Verlag, Berlin, 2019, pp. 176–184.
[25] A. Heinlein, A. Klawonn, and O. Rheinbach, *A parallel implementation of a two-level overlapping Schwarz method with energy-minimizing coarse space based on Trilinos*, SIAM J. Sci. Comput., 38 (2016), pp. C713–C747.
[26] A. Heinlein, A. Klawonn, and O. Rheinbach, *Parallel two-level overlapping Schwarz methods in fluid-structure interaction*, in Numerical Mathematics and Advanced Applications ENUMATH 2015, LNCSE 112, Springer-Verlag, Berlin, 2016, pp. 521–530.
[27] A. Heinlein, A. Klawonn, and O. Rheinbach, *Parallel overlapping Schwarz with an energy-minimizing coarse space*, in Domain Decomposition Methods in Science and Engineering XXIII, LNCSE 116, Springer-Verlag, Berlin, 2017, pp. 353–360.
[28] A. Heinlein, A. Klawonn, O. Rheinbach, and F. Röver, *A three-level extension of the GDSW overlapping Schwarz preconditioner in three dimensions*, in Domain Decomposition Methods in Science and Engineering XXV, LNCSE 138, Springer-Verlag, Berlin, 2019.
[29] A. Heinlein, A. Klawonn, O. Rheinbach, and O. Widlund, *Improving the parallel performance of overlapping Schwarz methods by using a smaller energy minimizing coarse space*, in Domain Decomposition Methods in Science and Engineering XXIV, LNCSE 125, Springer-Verlag, Berlin, 2019, pp. 383–392.
[30] T. Y. Hou and X.-H. Wu, *A multiscale finite element method for elliptic problems in composite materials and porous media*, J. Comput. Phys., 134 (1997), pp. 169–189.
[31] G. Karypis and V. Kumar, *A fast and high quality multilevel scheme for partitioning irregular graphs*, SIAM J. Sci. Comput., 20 (1998), pp. 359–392.
[32] H. H. Kim, E. Chung, and J. Wang, *BDDC and FETI-DP preconditioners with adaptive coarse spaces for three-dimensional elliptic problems with oscillatory and high contrast coefficients*, J. Comput. Phys., 349 (2017), pp. 191–214.
[33] A. Klawonn, M. Kühn, and O. Rheinbach, *Adaptive coarse spaces for FETI-DP in three dimensions*, SIAM J. Sci. Comput., 38 (2016), pp. A2880–A2911.

[34] A. Klawonn, M. Kühn, and O. Rheinbach, *Adaptive FETI-DP and BDDC methods with a generalized transformation of basis for heterogeneous problems*, ETNA, 49 (2018), pp. 1–27.
[35] A. Klawonn, P. Radtke, and O. Rheinbach, *A comparison of adaptive coarse spaces for iterative substructuring in two dimensions*, ETNA, 45 (2016), pp. 75–106.
[36] A. Klawonn and O. Rheinbach, *A parallel implementation of dual-primal FETI methods for three-dimensional linear elasticity using a transformation of basis*, SIAM J. Sci. Comp., 28 (2006), pp. 1886–1906.
[37] A. Klawonn and O. B. Widlund, *Dual-primal FETI methods for linear elasticity*, Comm. Pure Appl. Math., 59 (2006), pp. 1523–1572.
[38] J. Knepper, Adaptive Coarse Spaces for the Overlapping Schwarz Method and Multiscale Elliptic Problems, Ph.D. thesis, University of Cologne, Cologne, Germany, 2022.
[39] J. Mandel and B. Sousedík, *Adaptive selection of face coarse degrees of freedom in the BDDC and the FETI-DP iterative substructuring methods*, Comput. Methods Appl. Mech. Engrg., 196 (2007), pp. 1389–1399.
[40] J. Mandel, B. Sousedík, and J. Šístek, *Adaptive BDDC in three dimensions*, Math. Comput. Simulation, 82 (2012), pp. 1812–1831.
[41] L. Marcinkowski and T. Rahman, *Additive average Schwarz with adaptive coarse spaces: Scalable algorithms for multiscale problems*, ETNA, 49 (2018), pp. 28–40.
[42] C. Pechstein and C. Dohrmann, *Modern domain decomposition solvers—BDDC, deluxe scaling, and an algebraic approach*, slides to a talk at NuMa Seminar, JKU Linz, December 10, 2013, http://people.ricam.oeaw.ac.at/c.pechstein/pechstein-bddc2013.pdf.
[43] C. Pechstein and C. R. Dohrmann, *A unified framework for adaptive BDDC*, ETNA, 46 (2017), pp. 273–336.
[44] Y. Saad, *Iterative Methods for Sparse Linear Systems*, 2nd ed., SIAM, Philadelphia, 2003.
[45] R. Scheichl, P. S. Vassilevski, and L. T. Zikatanov, *Weak approximation properties of elliptic projections with functional constraints*, Multiscale Model. Simul., 9 (2011), pp. 1677–1699.
[46] B. Smith, P. Bjørstad, and W. Gropp, *Domain Decomposition: Parallel Multilevel Methods for Elliptic Partial Differential Equations*, Cambridge University Press, Cambridge, 1996.
[47] N. Spillane, V. Dolean, P. Hauret, F. Nataf, C. Pechstein, and R. Scheichl, *Abstract robust coarse spaces for systems of PDEs via generalized eigenproblems in the overlaps*, Numer. Math., 126 (2014), pp. 741–770.
[48] N. Spillane and D. Rixen, *Automatic spectral coarse spaces for robust finite element tearing and interconnecting and balanced domain decomposition algorithms*, Int. J. Numer. Methods Eng., 95 (2013), pp. 953–990.
[49] A. Toselli and O. Widlund, *Domain Decomposition Methods—Algorithms and Theory*, Springer Series in Computational Mathematics 34, Springer-Verlag, Berlin, 2005.